An Airborne X-band Synthetic Aperture Radar Receiver Design and Implementation

Ajmal Ismail Mohungoo

A dissertation submitted to the Department of Electrical Engineering,
University of Cape Town, in fulfilment of the requirements
for the degree of Master of Science in Engineering.

Cape Town, January 2004

Declaration

I declare that this dissertation is my own, unaided work. It is being submitted for the degree of Master of Science in Engineering at the University of Cape Town. It has not been submitted before for any degree or examination in any other university.

Signature of Author .....

Cape Town

January 21, 2004

Abstract

This dissertation focuses on the design and implementation of an X-band receiver for use in the *South Afican Synthetic Aperture Radar* (SASAR II) project. The SAR will be used to demonstrate the capability of building a high resolution X-band imaging radar in South Africa. The design starts by investigating the maximum power return from different targets over a swath width with changing incidence angles. A receiver-power-level table and diagram were constructed, with the power return from a trihedral corner reflector as maximum input power and thermal noise as the minimum input power to the receiver. The output of the receiver, which has to be fed to the input of an *analogue-to-digital converter* (ADC), is limited by the ADC's maximum operating input power. Amplifiers, attenuators and mixers were chosen to implement a dual-stage downconversion from a *radio frequency* (RF) of 9300 MHz to a 2^{nd} IF of 1300 MHz and then to a 1^{st} IF of 158 MHz. A *sensitivity time control* (STC) is implemented in the receiver to cater for the limited dynamic range of the ADC. The power return varies with range and hence, time. Thus, an STC will correct for low return power, at far range, by boosting the received signal and attenuating large return power, at close range, ideally providing a fairly constant power return at the receiver output. A *manual gain control* (MGC) is also needed in the receiver, such that none of the components are driven into saturation. The gain control is switched on when large targets are expected to fall in the swath width, otherwise it is switched to a minimum for targets with low backscattered power. The tests that were carried out on the receiver components showed that all the components operated very close to their specifications. The cascaded filters work well in tailoring the front-end 3-dB bandwidth to close to the required 3-dB bandwidth. The receiver was designed to have enough gain to boost the maximum power received to within the operating range of the ADC, without saturating any components in the receiver. The noise figure test showed a noise figure of 4.20 dB. This is 1.73 dB higher than the calculated noise figure of 2.47 dB which is a result of an underestimation of the losses in the system.

Acknowledgements

I would like to express my sincere gratitude to God Almighty for making this dissertation possible.

I am especially thankful to my supervisor, Professor Mike Inggs, for all his guidance, support and numerous technical input in shaping up this project from its embryonic stage to its final stage.

I am also indebted to Mr. Hannes Koetzer, from Reutech Radar System, for providing equipment, time and advice in the testing of the noise figure of the radar receiver and improving the design.

In addition, I wish to thank all the graduates in the Radar and Remote Sensing Group (RRSG) at UCT, especially Richard Lord and Thomas Bennett, for all their help and assistance in writing up this dissertation.

Finally, many thanks to my father Taleb, my mother Rookshanah and my sister Somayya for their love, support and encouragement during my studies.

Contents

List of Figures

List of Tables

List of Symbols

A_R	–	Antenna Area
A_e	–	Effective Antenna Area
A_c	–	Scattering Area of a target
d	–	Antenna Aperture length
A	–	Length of slotted waveguide antenna
B	–	Width of slotted waveguide antenna
B_r	–	Receiver Bandwidth
c	–	Speed of light
k	–	Boltzmann constant
f_{ADC}	–	Sample rate of Analog-to-Digital Converter
T_0	–	Noise Temperature of 290 K
T_s	–	System Noise Temperature
t_r	–	Rise time of receiver
R_r	–	Length of clutter strip
R	–	Range from antenna to target
G	–	Gain of antenna
p_{max}	–	Maximum power density
P_{tx}	–	Transmitted Power
P_{rx}	–	Received Power
L_s	–	System Losses from target to antenna output e.g. two way path loss, duplexer, TR cell
a	–	Length of trihedral corner reflector
β_s	–	Azimuth Beamwidth of a Synthetic Antenna
δR_{sr}	–	Slant Range Resolution
δR_{gr}	–	Ground Range Resolution
λ	–	Wavelength of carrier signal

θ – Incidence angle
ψ – Grazing angle
η – Angle off boresight axis
σ_t – Radar cross-section
σ° – Backscattering coefficient
τ – Pulse duration
γ – Normalised backscattering coefficient
ϕ_a – 3-dB azimuth beamwidth
ϕ_e – 3-dB elevation beamwidth

List of Acronyms

LNA	–	Low Noise Amplifier
LO	–	Local Oscillator
STALO	–	Stable Local Oscillator
IF	–	Intermediate Frequency
TOI	–	Third Order Intercept
MCG	–	Manual Gain Control
STC	–	Sensitivity Time Control
ADC	–	Analogue-to-Digital Converter
SAR	–	Synthetic Aperture Radar
PRF	–	Pulse Repetition Frequency
SPDT	–	Single Pole Double Throw
UAV	–	Unmanned Aerial Vehicles
SMA	–	SubMiniature version A
TR	–	Transmit-receive

Nomenclature

Azimuth—Angle in a horizontal plane, relative to a fixed reference, usually north or the longitudinal reference axis of the aircraft or satellite.

X-band—Frequency range from 8 GHz to 12.5 GHz.

Baseband—The range of frequencies occupied by the signal before modulation or after demodulation close to dc.

Beamwidth—The angular width of a slice through the mainlobe of the radiation pattern of an antenna in the horizontal, vertical or other plane.

Boresight— The axis of symmetry of the beam of an antenna.

Complex Sampling—The sampling of the basebanded I & Q channel.

Doppler frequency—A shift in the radio frequency of the return from a target or other object as a result of the object's radial motion relative to the radar.

Insertion loss—The difference in dB power measured at the component input and output.

Ground Range—The slant range projected on the ground

Slant Range—The radial distance from a radar to a target.

S**ynthetic Aperture Radar** (**SAR**)—A signal-processing technique for improving the azimuth resolution beyond the beamwidth of the physical antenna actually used in the radar system. This is done by synthesizing the equivalent of a very long sidelooking array antenna

Scatterometer—A microwave remote sensing device used to measure the backscatter return off the ocean.

Scattered—Denotes all energy that is not absorbed

Swath—The area on earth covered by the antenna signal.

Target—Any reflecting object which interferes with the transmitted wave and reflects part of its energy.

Chapter 1

Introduction

1.1 Background

This dissertation describes the design and implementation of an X-band *synthetic aperture radar* (SAR) receiver for the SASAR II system. Synthetic Aperture Radar is a technique that provides high resolution images of extensive areas of the Earth's surface from a platform operating at long ranges irrespective of weather conditions or darkness [6]. The first experimental demonstration of SAR occurred in 1953 when a stripmap of a section of Key West, Florida was generated at 3 cm wavelength by a group from the University of Illinois [22].

1.2 Overview of SASAR II project

Synthetic Aperture mapping by airborne or spaceborne radar is achieved "*by the coherent processing of reflectivity data collected from the earth's surface over relatively wide bandwidths at shifting angles presented during illumination* [22]".

SASAR II is an airborne X-band SAR that is due to fly in March 2004 as a demonstration of the capability to design and build a high resolution X-band imaging radar. As a first step towards building the SASAR II system, SunSpace, forming part of a consortium, launched a SAR Technology Project. The aim of this consortium is to consolidate and develop the South African SAR capability with SunSpace ability to deploy these systems on satellites and UAV platforms. The consortium commissioned the *Radar and Remote Sensing Group* (RRSG) at the University of Cape Town to design and implement a SAR radar to demonstrate local capability. The technical capability and manpower development of the RRSG is considered core to the success of this initiative.

1.3 Motivation

A synthetic aperture radar achieves high resolution and it performs equally well at night, through haze, cloud and rain. Its use has been demonstrated in diverse applications: ice monitoring, monitoring agriculture, mapping, resource management and law enforcement [25]. Low frequencies SAR have particular advantages in the fact that electromagnetic waves penetrate more than higer frequencies through foliage and buried targets and this is of particular advantage to the mining industries.

1.4 User Requirements

The following user requirements were specified for the receiver of the SAR system by the system engineer:

- The system should have a nominal square pixel resolution of about $2 \times 2\,[\mathrm{m}]$.
- The transmitted power and carrier frequency are set considering the operational parameters of the available power amplifier.
- The transmitted power is 3.5 kW.
- The transmitted carrier frequency is set to 9.3 GHz .
- A platform height of 3 km above sea level.
- Maximum number of range samples of 8192.
- The swath width should be determined by the selected number of range samples, the slant range resolution and incidence angle.
- Maximum instantenous receiver bandwidth of the system should be 100 MHz.
- The system shall have a near incidence angle of 40°.
- The antenna beamwidth should be 30° in elevation and 3° in azimuth.
- The system shall have 2 IF stages at 158 MHz and 1300 MHz respectively and an RF stage at 9300 MHz.
- System filtering should ensure maximum phase linearity.
- An *analogue-to-digital converter* (ADC) with sample rate of 210 MHz and a minimum of 8 bits and with maximum input power of 13 dBm should be used to digitise the received signal.

- The transceiver shall have switchable gain i.e. both manual and automatic gain.
- *Sensitivity Time Control* (STC) capability should be implemented in the system.
- The system shall be built with extensive Built-in Test (BIT) capabilities to allow for preflight testing in the laboratory.
- The system shall be designed with default operating mode i.e. function in the receiver mode and not in BIT mode.

1.5 Overview of the Thesis

The dissertation starts with an overview of synthetic aperture radar in Chapter 2. In this chapter, the theory that is used to design the system is explained. The derivations of the terms and formulas used in the following chapters are presented here. Section 2.2 describes the pulsed radar concept with an explanation of the radar equation. The centre frequency used is important in choosing the size of the antenna and the depth of radar penetration required in this project. The beamwidth relates to the swath width, antenna gain and hence antenna size. Section 2.3 introduces the SAR concepts, vital in designing the receiver, with reference to the geometry of the airborne radar configuration. Azimuth compression in SAR, is used to boost the signal power of a point-like target over noise. Finally, an explanation of the relationship between the PRF and doppler bandwidth is provided.

In Chapter 3 the front-end power return of SASAR II radar is discussed. The terms and theory developed in Chapter 2 are used in the radar equation. Two types of targets are considered namely point targets and distributed targets. The corner reflector at RRSG-UCT is used to estimate the power return of large point-like targets. Figure 1.1 shows the mainbeam setup of the antenna pointing to the Earth with the boresight axis closer to the near-swath. Two gain pattern simulations have also been investigated namely *cosecant-squared* and *sinc-squared* antenna pattern as explained in Section 3.4. The latter proved to be the more appropriate one in providing the highest gain. Section 3.5 describes the distributed targets used in the design, such as trees and wheat fields and are chosen from models described by Ulaby [15]. Point-like targets are also expected to be present in the swath width and their radar cross section are calculated in Section 3.5.3. The backscattered power is simulated at the front-end of the antenna as described in Section 3.6 for varying terrain types and point targets that the radar might encounter. The design also includes the different scenarios with the boresight axis of the antenna at near-swath, mid-swath and far-swath. The incidence angle used for near-swath is set to 40° relating to a

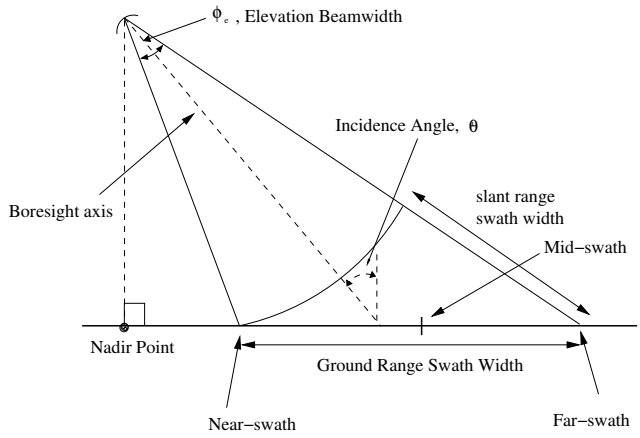

Figure 1.1: Side Geometry with the 3-dB Beamwidth Covering the Swath Width.

maximum ground range of 11513 m for 8192 range bins. The bandwidth of the system used in simulation for the front-end was set to 200 MHz and tailored to reach 100 MHz as explained in Chapter 4.

The receiver is broken down into 2 *intermediate frequencies* (IFs) stages and a *radio frequency* (RF) stage as shown in Figure 1.2. The particular IFs were chosen to match those frequencies of previous projects such that future expansion of the system could be performed. Chapter 4 describes the RF and IF stages of the receiver. The use of a dual conversion receiver is required to relieve the streneous cut-off required for the RF filter in order to attenuate the image frequency response to a minimum. A justification of the different components used is laid out in this chapter and the transfer function of the system is worked out. The theory and properties associated with the components are investigated. The *low noise amplifier* (LNA) is used in the front end of the system to set the noise figure of the receiver as is described in Sections 4.2 and 4.4. Simulations are done with varying gains so as not to saturate the components in the later stages of the receiver and a maximum gain of 22 dB is selected. The use of the image rejection filter in the RF stage is explained in Section 4.5. Section 4.6 deals with mixers, conversion loss and intermodulation distortions. The relative output of the 2 mixers, which consists of the RF and spurious responses, are displayed. Section 4.7 shows plots of the transfer function of the IF filters used in rejecting out-of-band signals.

A *sensitivity time control* (STC) is implemented using an electronic attenuator and gain blocks as explained in Section 4.8. To prevent the receiver from being overloaded by strong echoes from nearby terrains, objects and targets, the STC is used to lower the gain for the early part of the interpulse period and gradually increases the gain for the return from the far range. This in effect causes the return power to be fairly constant over the interpulse period. From simulations performed in Chapter 3, an attenuator of 20 dB

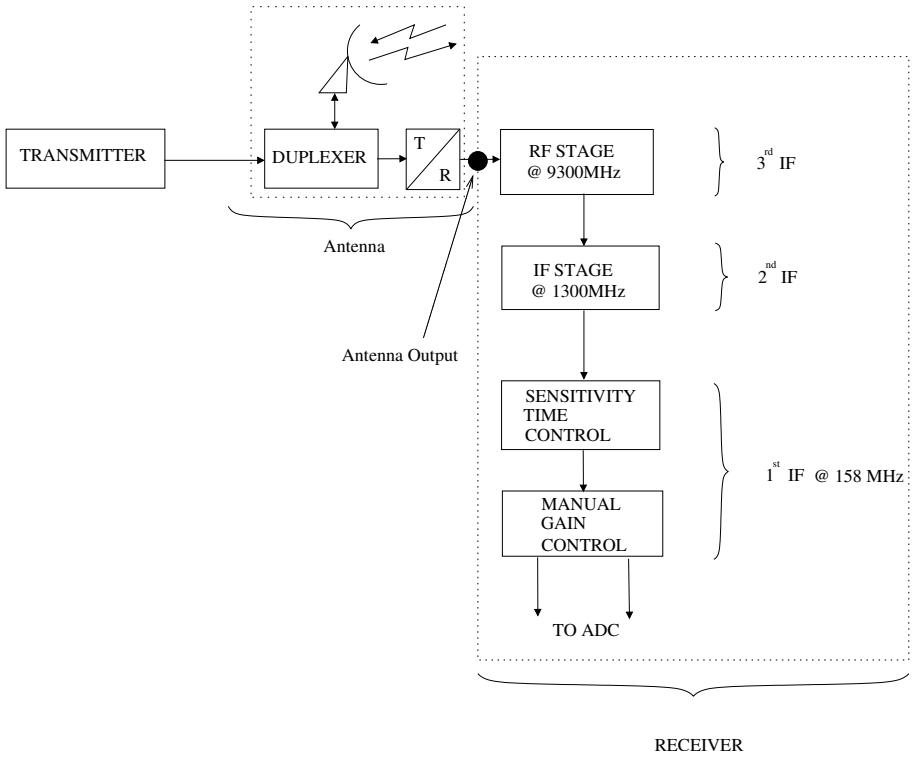

Figure 1.2: Receiver Block Diagram

dynamic range should suffice.

The MGC is a user-switchable gain. The implementation using a digital attenuator is also described in Section 4.8. Its main function is to switch the gain to different user-defined values depending on the terrain being imaged. From the receiver level tables of Section 4.11 and simulations of maximum return signal and noise level, an attenuation of dynamic range of 30 dB is required.

The receiver-power-level table and the receiver-power-level diagram are two important tools in designing and implementing a receiver such that no components are driven into saturation thereby generating harmonics. With an 8-bit *analogue-to-digital converter* (ADC) of peak voltage of 1 V, the maximum instantaneous power input is 13 dBm. The maximum power return from large targets, as modelled in Chapter 3, is -55.3 dBm and hence, a 60 dB gain receiver is designed to boost the signal input up to a maximum of 7 dBm. For an antenna facing a blackbody, which is the Earth for this project, the noise temperature is $290\,\mathrm{K}$. The thermal noise is thus calculated at the antenna output and is tracked down the receiver together with noise generated by the different components like the LNA, mixers, IF amplifiers and attenuators. The theoretical receiver noise temperature is worked out to be a minimum of $222\,\mathrm{K}$ from the available specifications of the individual components with attenuation being at its minimum.

The largest power return and noise level at the front-end of the receiver predicts a dynamic range of 40 dB. Amplification is required to boost the signal but at the same time noise generated by the system has to be taken into account and ways of limiting this noise are discussed. The mixers, filters and amplifiers used are justified in this chapter. Intermodulation products are investigated together with the effects of image frequency contribution in undermining the system.

Chapter 5 lays out the different tests that are performed on the IFs of the receiver. The tests are performed on each of the 4 sections namely,

1. 3^{rd} IF (RF stage or 3^{rd} IF)
2. 2^{nd} IF (L-band stage or 2^{nd} IF)
3. 1^{st} IF (1^{st} IF STC)
4. 1^{st} IF (1^{st} IF MGC)

The gain, insertion loss tests are performed on each stage individually and the output spectrum is mesaured for different frequency of interest. The insertion loss tests basically ascertain that no components are driven into saturation. A signal is injected, at a power level designed in the receiver-level table for minimum MGC attenuation, in each of the four sections and the output is measured and compared with the expected output. Varying the frequency of the input signal helps in testing the cut-off of the filters in the different sections.

Noise figure tests are performed on the system as a whole for minimum and maximum attenuation of the MGC attenuator in Section 5.7 and the output power level of the signal at band centre versus signal on either side is measured in Section 5.8.

Chapter 6 gives the conclusions and recommendations for future work on the receiver based on the design and tests performed. The receiver works according to the design. The simulated power return for a corner reflector is -55.3 dBm. The components are not driven into saturation when a signal of -50 dBm is injected at the front-end of the receiver. The cascaded filters result in a 3-dB bandwidth of 94 MHz at the ADC input.

Chapter 2

Theory of Airborne SAR

2.1 Introduction

The theory underlying the development of the Airborne SASAR II system is explained in this chapter. The analysis of the terms used in the design of the radar receiver is presented, as they appear in the radar equation, which remains fundamental to radar design. Section 2.2 introduces the concept related to pulse radar with the properties of a radar that affect transmission of a pulse. Section 2.3 lays out the basics of SAR, with an explanation of the parameters crucial to the radar receiver design. An important characteristic of a SAR image is its resolution, which is defined in terms of minimum distance at which two closely spaced scatterers of equal strength may be resolved. SAR and conventional radar achieve slant range resolution in a similar way by using pulse-ranging technique. However, SAR is distinctive in achieving along-track (azimuth) resolution by using aperture synthesis and is defined in terms of the antenna dimension only.

2.2 Pulsed Radar Basics

The detection range of a radar system is primarily a function of three variables, namely:

1. Transmitted Power.
2. Antenna Gain.
3. Receiver Sensitivity.

An increase in transmitted power will increase the amount of energy radiated and hence, the backscattered power from the target will be stronger. The antenna gain is a measure of

the radiated energy towards the target as opposed to uniform radiation of energy. Receiver sensitivity is a measure of the capability of the receiver in detecting target returns.

2.2.1 Antenna Gain

Antenna gain describes the degree to which an antenna concentrates electromagnetic energy in a narrow angular beam. The two parameters associated with the gain of an antenna are the directive gain and directivity. The gain of an antenna serves as a figure of merit relative to an isotropic source with the directivity of an isotropic antenna being equal to 1 by definition [14].

The directive gain, G, of an antenna at a far-field distance, R, is defined as the ratio [7, pg6.3],

$$\begin{aligned} G &= \frac{\text{maximum radiation intensity}}{\text{average radiation intensity}} \\ &= \frac{\text{maximum power per steradian}}{\text{total power radiated}/4\pi} \end{aligned}$$

The far-field region is assumed in this project unless otherwise stated and is the region defined by the inequality [14, pg72],

$$R \geq \frac{2d^2}{\lambda} \tag{2.1}$$

where d is the antenna aperture length.

This ratio can also be expressed in terms of maximum radiated power density $\left(\frac{\text{W}}{\text{m}^2}\right)$ at a far-field distance, R, over the power density radiated by an isotropic source at that same distance,

$$\begin{aligned} G &= \frac{\text{maximum power density}}{\text{total power radiated}/4\pi\text{R}^2} \\ &= \frac{\text{P}_{\text{max}}}{\text{P}_{\text{rad}}/4\pi\text{R}^2} \end{aligned} \tag{2.2}$$

Equation 2.2 shows how much stronger the actual maximum power density is, than it would be if the radiated power was distributed isotropically.

The directivity, D_{max}, is defined as the value of the directive gain in the direction of its maximum value [14, pg77].

The gain of an antenna is related to the directivity is given by,

$$G = \epsilon D_{max} \tag{2.3}$$

The radiation efficiency, ϵ, is given by,

$$\epsilon = \frac{P_{rad}}{P_{tx}} = \frac{P_{tx}}{P_{tx} + P_{loss}} \tag{2.4}$$

where P_{tx} is the power coupled into the antenna and P_{rad} being the actual power being radiated.

2.2.2 Antenna Radiation Pattern

The gain of an antenna also varies with the type of antenna pattern as explained in [10, pg29]. It relates the distribution of electromagnetic energy in angular space. For a pencil beam antenna with a *sinc-squared* pattern, the normalized power radiation pattern in azimuth direction, ϕ, is given by,

$$|E(\phi)|^2 = \left[\frac{sin\left[\left(\frac{\pi d}{\lambda}\right) sin(\eta)\right]}{\left(\frac{\pi d}{\lambda}\right) sin(\eta)} \right]^2 \tag{2.5}$$

where η is the angle off boresight.

The directive gain of an antenna can also be expressed in terms of its physical dimension. The aperture of an antenna is equal to its physical area projected on a plane orthogonal to the direction of the mainbeam. The directive gain is given in [7] by,

$$G = \frac{4\pi A_e}{\lambda^2} \tag{2.6}$$

where A_e is the effective aperture.

The derivation of Equation 2.6 to calculate antenna gain is explained in [6, pg9]. The 3-dB (half-power) beamwidth of an antenna with aperture size, d, is given in [10] by,

$$\phi = \frac{0.88\lambda}{d} \tag{2.7}$$

$$\approx \frac{\lambda}{d} \text{[radians]} \tag{2.8}$$

Figure 2.1 shows the "$\left(\frac{sin(x)}{x}\right)^2$" antenna pattern for a pencil beam antenna with the a 3 dB beamwidth of 6°.

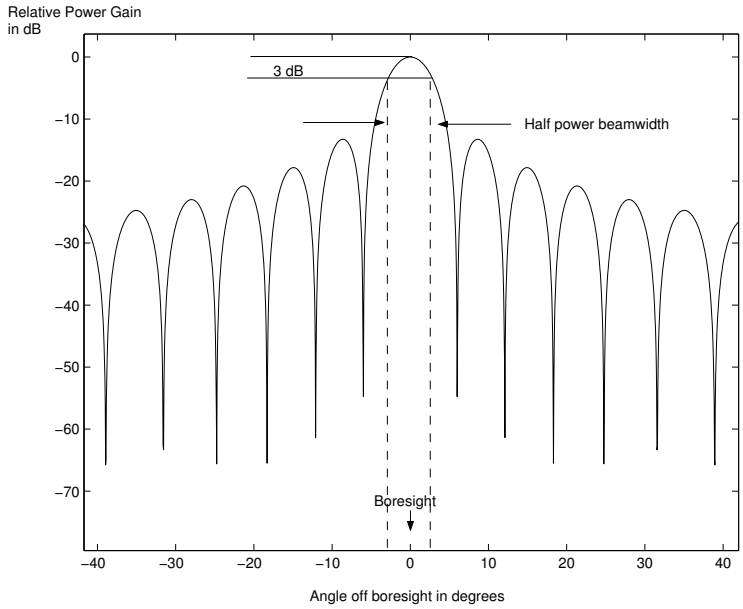

Figure 2.1: Radiation Pattern of an Antenna with 3 dB Beamwidth of 6°.

2.2.3 Radar Cross Section

The *radar cross section* (RCS) describes the apparent area of the target as perceived by the radar and is a measure of how much power flux is intercepted by the target and re-radiated towards the radar [6]. As a measure of the return power at the front end of the receiver, different targets are used here to simulate the ground return. The targets can be categorized under two types namely [15, pg18],

- Distributed Targets

  Modelled as an ensemble of scattering centres randomly distributed in spatial position over the illuminated area.

- Point Targets

  Targets that scatter incident power almost uniformly with incidence angle.

A distributed target consists of a large number of randomly distributed scatterers. When it is illuminated by a coherent electromagnetic wave, the magnitude of the scattered signal is equal to the phasor sum of all the returns from all of the scatterers illuminated by the incident beam [15].

The RCS, σ_t, for a distributed target is defined as,

$$\sigma_t \quad = \quad \sigma^{\circ}(\theta) \times A_c[\mathrm{m}^2] \tag{2.9}$$

where $\sigma^{\circ}(\theta)$ is the backscatter coefficient, as explained in Section 2.2.4, and A_c represents the clutter area. Figure 2.2 shows the scattering area, A_c, within the 3 dB beamwidth of the radar.

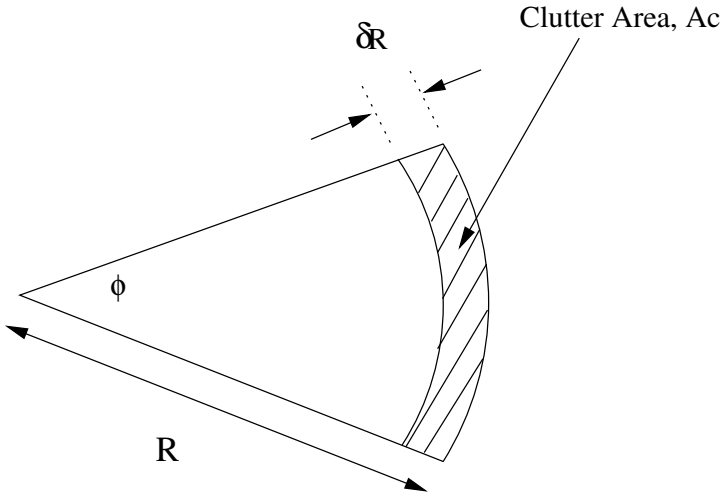

Figure 2.2: Clutter Area in Azimuth Beamwidth and Pulse Duration Projected on the Ground.

2.2.4 Backscattering Coefficient σ°

The backscattering coefficient, σ°, used in Equation 2.9, is the radar cross section of a small increment of ground area, ΔA, and defined from [16] by,

$$\sigma_m^0 = \Sigma_{n=1}^{N} \frac{\sigma_n}{\Delta A} [\mathrm{m}^{-2}] \tag{2.10}$$

It defines an average radar cross section per unit area or the RCS of a distributed target of horizontal area A, normalized with respect to A. A reflector which concentrates its reflected energy over a limited angular direction may have an RCS for a particular direction which exceeds its projected area and hence backscattering coefficient and RCS are quoted with aspect angle.

2.2.5 The Radar Equation

The radar equation relates the important parameters affecting the received signal of a radar. The derivation is explained in many texts, namely [6, pg11], [10, pg5], [12, pg7] and [14, pg198]. Figure 2.3 shows the backscattered power from a target with radar cross section, σ_t, at a range, R. The radar equation relating the range from the target to the

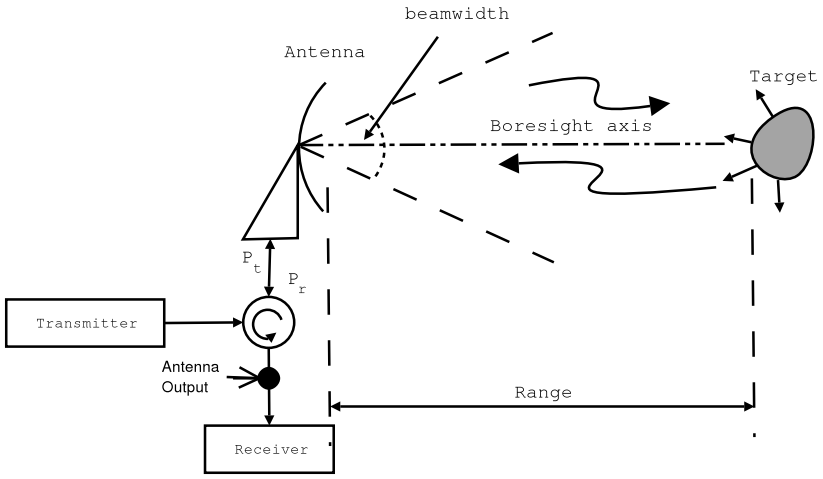

Figure 2.3: Radar Backscatter From a Target.

radar is given by,

$$P_{rx} = \frac{P_{tx} G^2 \lambda^2 \sigma_t}{(4\pi)^3 R^4 L_s} \text{[W]} \tag{2.11}$$

where L_s is the system losses. The radar equation is used to simulate the return power at the antenna output such that the maximum input power to the receiver is known.

2.3 SAR Basics

The platform on which the SAR is mounted is usually an aircraft or satellite. Figure 2.4 shows the stripmap SAR geometry and radar position relative to the ground. A burst of pulses is transmitted by a side-looking antenna pointed towards the ground and the backscattered power is collected with the signal corresponding to each pulse. The SAR system saves the phase histories of the responses at each position as the real beam moves past and then, in post processing it weighs, phase shifts and sums them up to focus on one point target (resolution element) at a time and suppresses all others.

2.3.1 Receiver Bandwidth

An important aspect in designing a radar is the radar bandwidth, B_r. In conjuction with SAR, bandwidth will essentially mean the range of frequencies over which the target reflectivity data are collected. The receiver bandwidth is determined by the bandwidth of the transmitted pulse . The half power bandwidth of the radar receiver is the range of frequencies up to the point where the frequency response drops to half of its maximum and is known as the 3-dB bandwidth. The radar 3-dB bandwidth is related to the pulse

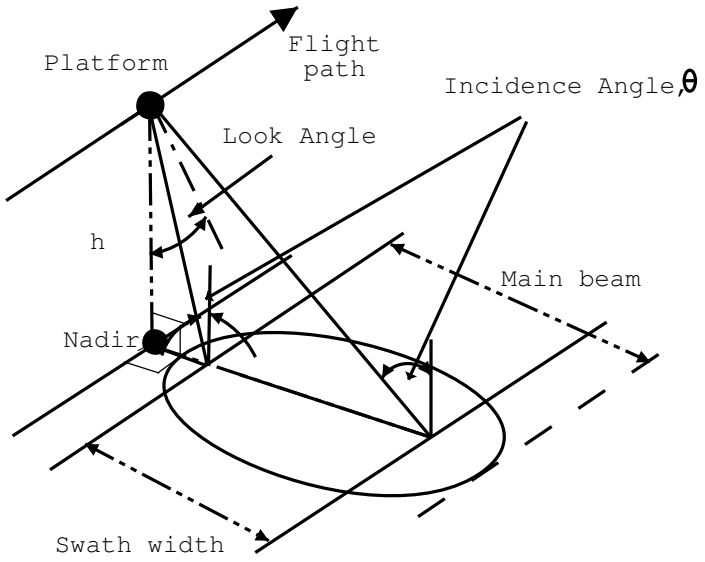

Figure 2.4: Geometry of stripmap SAR.

duration and given by [10, pg92],

$$B_r = \frac{0.886}{\tau} \approx \frac{1}{\tau} \tag{2.12}$$

2.3.2 Doppler Bandwidth

As the radar moves past the point targets at point B and D, as shown in Figure 2.5, the doppler shift will vary approximately linearly with time, passing the zero frequency at boresight for zero squint. This Doppler shift approximates to a linear chirp. Azimuth compression can be thought of as the compression of the Doppler signal produced during the integration length, $R\phi_a$. The Doppler bandwidth consists of the frequencies produced, as a result of scatterers falling in the beamwidth of the radar, as the platform moves past the targets. The Doppler bandwidth, for a narrow azimuth beamwidth, is thus given by [22, pg272],

$$f_{d2} - f_{d1} = \frac{2v_p\phi_a}{\lambda} \tag{2.13}$$

where v_p is the platform ground velocity and ϕ_a is the 3-dB beamwidth.

Nyquist sampling in SAR mode requires that,

$$PRF \geq \frac{2v_p\phi_a}{\lambda} \tag{2.14}$$

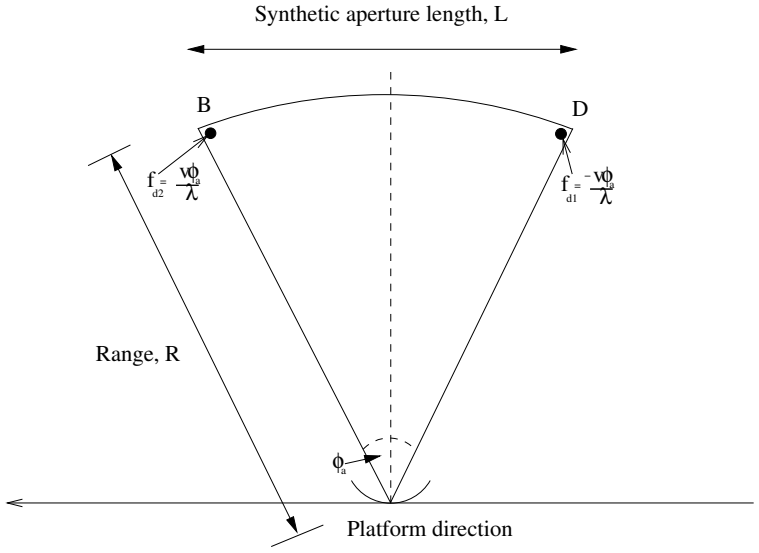

Figure 2.5: Stationary Point Targets in a Moving Radar Beam.

setting a minimum PRF such that the cross range data is not undersampled and aliased in processing.

2.3.3 Resolution

The range resolution can be defined as the separation between targets before they can be seen as two independent targets rather than one [6]. A SAR resolution element is defined in terms of both the slant range resolution and the azimuth range resolution.

Slant Range Resolution

To meet the Nyquist criteria each echo produced from a pulse of bandwidth, B_r, has to be sampled by at least B_r complex samples per second.The slant range resolution is defined in terms of the time delay between the echoes from two targets whereby if the time delay, τ_d, is greater that the pulse duration, τ, then the two targets are "seen". If the targets are closer than the pulse length, τ, then the echoes merge. Figure 2.6 shows the range resolution of a radar from 2 consecutive pulses. From Figure 2.6a, the two targets are easily resolved when they are more than a pulse length apart. They become unresolvable when they are less than a pulse length apart as can be seen in Figure 2.6b and just resolvable when they are separated by a pulse length as shown in Figure 2.6c.

The slant range resolution is given by [9],

$$\delta R_{sr} = \frac{c\tau}{2} \tag{2.15}$$

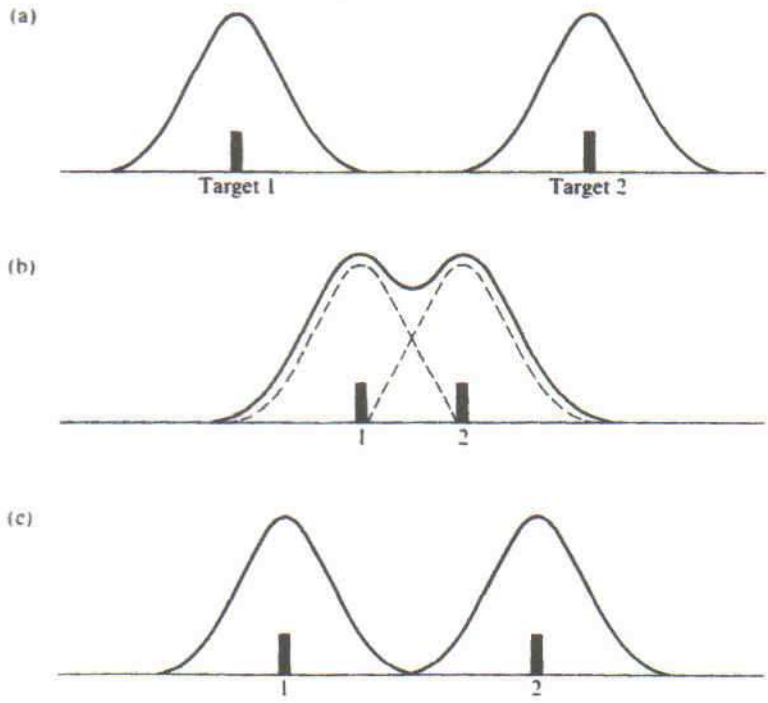

Figure 2.6: Resolution of Two Pulses [6].

Translation to the ground plane as shown in Figure 2.7 gives,

$$\delta R_{gr} = \frac{c\tau}{2\,sin\,(\theta_i)}$$

Unambiguous data sampling of the slant range requires that,

$$f_{ADC} \geq B_r \tag{2.16}$$

where f_{ADC} is the complex sampling frequency.

Azimuth Resolution

The azimuth resolution depends on the azimuth beamwidth. The SAR antenna beamwidth differs from real antenna beamwidths in the fact that two-way propagation is required before the synthetic antenna is formed [6]. The azimuth beamwidth of the SAR is derived from the synthetic aperture length, L, referring to Figure 2.5,

$$L = R\phi_a \tag{2.17}$$

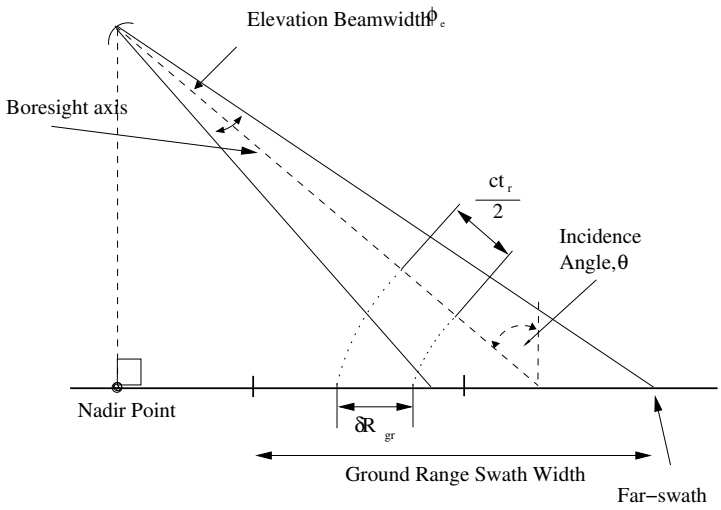

Figure 2.7: Radar Scene Geometry

where the 3-dB azimuth beamwidth, ϕ_a, is approximately given by,

$$\phi_a = \frac{\lambda}{d} \tag{2.18}$$

The synthetic aperture length can be written as,

$$L = \frac{R\lambda}{d} \tag{2.19}$$

The beamwidth of the SAR antenna is given by [6],

$$\beta_s = \frac{\lambda}{2L} = \frac{d}{2R} \tag{2.20}$$

where the factor "2" comes from the signal processing manipulation as explained in [26, pg9]. The spatial resolution on the ground is the product of the angular resolution and the range and is given by,

$$\delta R_a = R\beta_s = \frac{d}{2} \tag{2.21}$$

This equation does not account for processing weighting factors which affect both azimuth and range resolution.

2.3.4 Pulse Repetition Frequency (PRF)

The PRF of the SAR system is the number of pulses that are transmitted per second. It has an important implication on the rate of data that must be recorded and as far as the receiver is concerned it dictates the average power which is given by,

$$P_{ave} = P_{tx} \times \tau \times PRF \tag{2.22}$$

The minimum PRF is set according to Equation 2.14 while the maximum is set by the maximum unambiguous range of the radar among others. A monostatic radar can only sample backscatter power between two successively transmitted pulses from a range R. The time delay required between transmission of two pulses in succession is given by,

$$T \geq \frac{c}{2R}$$

This leads to a maximum PRF for unambiguous range given by,

$$\begin{aligned} PRF_{max} &= \frac{1}{T} \\ &= \frac{2R}{c} \end{aligned} \tag{2.23}$$

Chapter 3

Return Power Simulation

3.1 Introduction

The system design consists of iterations such that the user requirements are met. It involves the simulations of the power return at the antenna output with the losses due to the duplexer, *transmit-receive* (TR) cell and two-way path, being taken into account in the radar equation. The antenna gain pattern and the antenna efficiency designed in Section 3.4, is used in the received power calculation. Section 3.5 describes the types of terrain used in the simulation of backscattered power with the inclusion of point-like targets. The RCS of distributed targets are modelled statistically while that of point-like target are inferred from Skolnik [13]. The boresight axis is varied in its position on the swath width to investigate the relation between the antenna gain and the propagation attenuation as performed in the simulations in Section 3.6.

3.2 Design Parameters

Figure 3.1 shows a typical receiver up to the *analogue-to-digital converter* (ADC). The system is designed with BIT capabilities as shown with test-signal injection points. This would allow the testing of the different paths in the receiver separately by use of switches and with the test signals being fed from the transmitter. In designing the receiver for the airborne SASAR II system, certain values were obtained from the system design document [4]. Table 3.1 shows the assumptions made in order to get an idea of the realistic values in the simulations carried out.

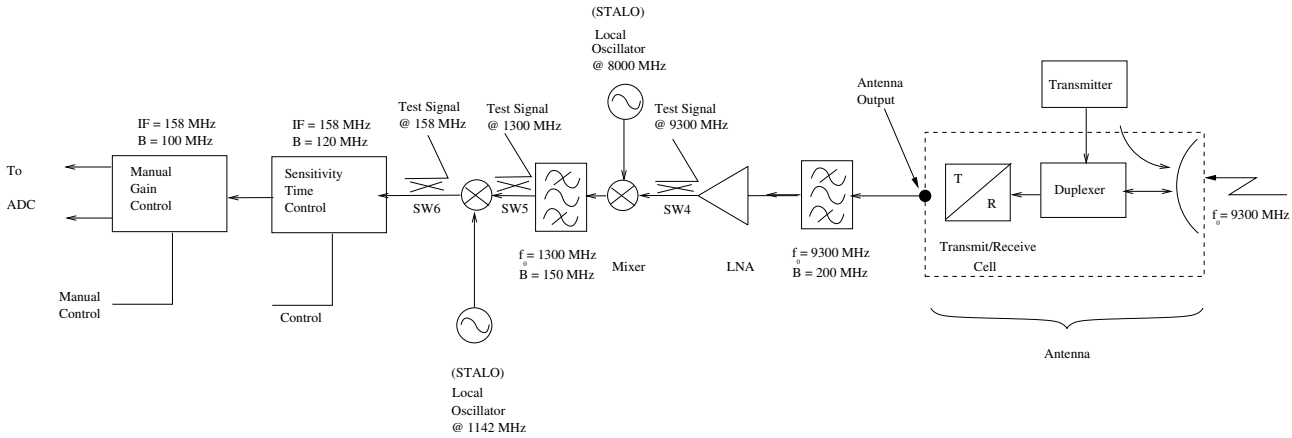

Figure 3.1: Receiver Block Diagram.

Table 3.1: User-Defined Parameters.

Transmitted Power	3.5 kW
Altitude	3000 m
Slant Range Resolution	2 m
Pulse length	5 μs
Time Bandwidth product	27 dB

3.3 Bandwidth

To achieve high resolution a large bandwidth is required. From Section 2.3.3 of Chapter 2, the slant range resolution is given by,

$$\delta R_{sr} = \frac{c}{2B_r} \tag{3.1}$$

For a 2 m slant range resolution this results in a bandwidth of

$$2 = \frac{c}{2B_r} \tag{3.2}$$

$$B_r = 75\,[\text{MHz}] \tag{3.3}$$

As specified in the user requirement and also, to limit the effect that processing weighting has on resolution, the end bandwidth of the receiver is chosen as 100 MHz. The front-end bandwidth is set to 200 MHz and tailored down by a series of cascaded filters to 100 MHz to relieve the filter transfer function as explained in Chapter 4.

Figure 3.2 shows the variation of slant range resolution with bandwidth. A 1.5 m resolu-

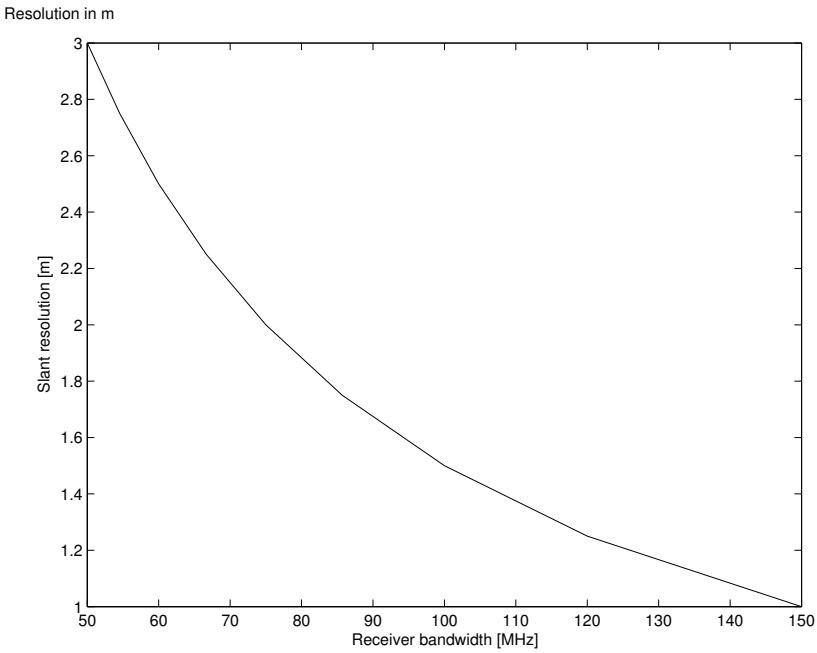

Figure 3.2: Resolution with 3-dB Receiver Bandwidth.

tion will theoretically be achieved with a 3-dB bandwidth of 100 MHz.

3.4 Gain

The antenna gain being one of the parameters determinant in the radar equation, is chosen as large enough as possible to increase the backscattered power intercepted. The design includes two antennas of possible use considering their shape and size.

3.4.1 Power Gain for Parabolic Dish

Assuming a dish diameter of 1 m and a 60% efficiency, the gain of the antenna is given by [6],

$$G = \frac{4\pi A_R}{\lambda^2} \tag{3.4}$$

$$= \frac{4\pi.(\pi.0.5^2.0.6)}{0.032^2} \tag{3.5}$$

$$= 5783 \tag{3.6}$$

$$= 37.6\,[\text{dB}] \tag{3.7}$$

where $A_R = \pi(\frac{d}{2})^2$.

3.4.2 Power Gain for Slotted Waveguide Antenna

The slotted waveguide antenna from JRC (from the UCT-RRSG microwave laboratory) or a similar antenna is another option. Table 3.2 shows the antenna specifications.

Table 3.2: Properties of JRC antenna.

Azimuth beamwidth	3.8^0
Elevation beamwidth	25^0
Operating Frequency	9300MHz
Length A	60cm
Width B	7cm

where A and B are shown in Figure 3.3.

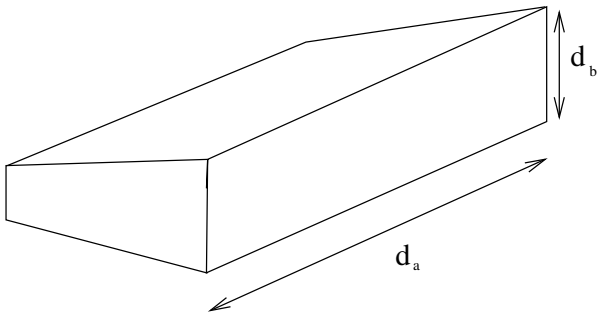

Figure 3.3: Waveguide Antenna Dimensions.

The power gain for such an antenna, with 50% efficiency, is given by [14, pg88],

$$G = 10log_{10}\left(\frac{4\pi d_a d_b}{\lambda^2}\right) \quad (3.8)$$

$$= 10log_{10}\left(\frac{4 \times \pi \times 0.6 \times 0.07}{0.032^2}\right) \quad (3.9)$$

$$= 27.1\,[\text{dB}] \quad (3.10)$$

3.4.3 Antenna Radiation Pattern

The sinc-squared antenna pattern is used to model the radiation pattern due to its larger gain as compared the cosecant-squared antenna pattern. A plot of the radiation pattern of the antenna, in elevation angle, with a 3-dB elevation beamwidth antenna of 30°, is shown in Figure 3.4.

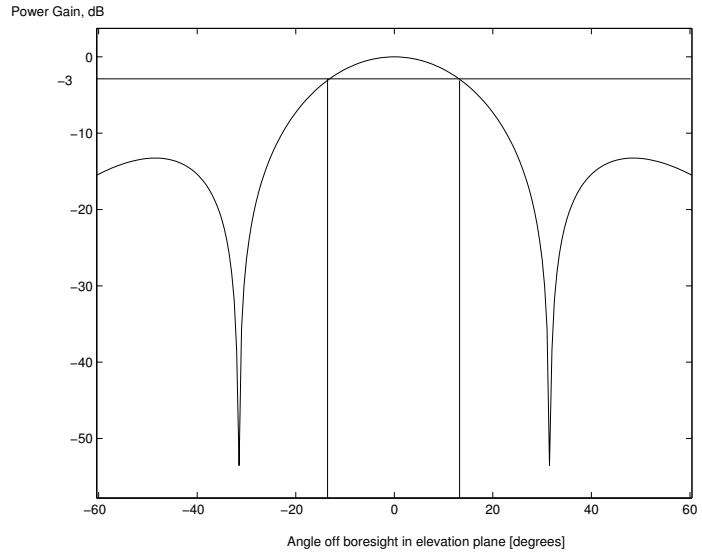

Figure 3.4: Elevation Antenna Pattern.

From the simulations of swath width, a 3-dB elevation beamwidth[1] of 37.8° is required to illuminate 8192 range bins at 40° of near incidence angle. An approximation to the gain for an antenna with an azimuth beamwidth of 6°, is calculated to be [6],

$$G \approx \frac{4\pi}{\phi_a \phi_e} \tag{3.11}$$

$$= \frac{4\pi}{6 \times 37.8} \tag{3.12}$$

$$= 22.6\,[\text{dB}] \tag{3.13}$$

where ϕ_a and ϕ_e are the 3-dB beamwidth in the azimuth and elevation plane respectively. In the actual simulation of the return power, a 3° azimuth beamwidth and 30° elevation beamwidth were used. From Equation 2.8, the length, d_a, and width, d_e, is calculated as follows,

$$d_a = \frac{\lambda}{\phi_a} \tag{3.14}$$

$$= \frac{0.0322}{3} \times \frac{180}{\pi} \tag{3.15}$$

$$= 0.617\,[\text{m}] \tag{3.16}$$

[1]The beamwidth was calculated using *Matlab* simulations for the return power with near-incidence angle at 40° . See Appendix C.

$$d_e = \frac{\lambda}{\phi_a} \tag{3.17}$$
$$= \frac{0.0322}{30} \times \frac{180}{\pi} \tag{3.18}$$
$$= 0.0617\,[\text{m}] \tag{3.19}$$

Hence, from Equation 2.6 the gain of the slotted-waveguide antenna, with 60% efficiency, is given by,

$$G = \frac{4\pi \times d_a \times d_e \times 0.6}{\lambda^2} \tag{3.20}$$
$$= \frac{4\pi \times d_a \times d_e \times 0.6}{0.0322^2} \tag{3.21}$$
$$= 295.05 \tag{3.22}$$
$$= 24.7\,[\text{dB}] \tag{3.23}$$

3.4.4 Cosecant-Squared Antenna Pattern

A different option for the antenna pattern is the cosecant-squared pattern, where the received power from a target at constant altitude, h, stays constant independent of range as shown in Figure 3.5. The gain pattern is given by [10, pg35],

$$G(\phi) = G(\phi_\circ)\frac{csc^2\phi}{csc^2\phi_\circ} \tag{3.24}$$

where the limit is given by,

$$\phi_\circ \leq \phi \leq \phi_1$$

with $\phi_\circ$ is the fan beamwidth and ϕ_1 is the end limit of the cosecant beam.

The derivation of the received power for an antenna having a cosecant-squared beam is given as follows:

The received power, P_{rx}, can be represented by,

$$P_{rx} = K\frac{G^2(\phi)}{R^4} \tag{3.25}$$
$$= K_1\frac{csc^4\phi}{R^4} \tag{3.26}$$

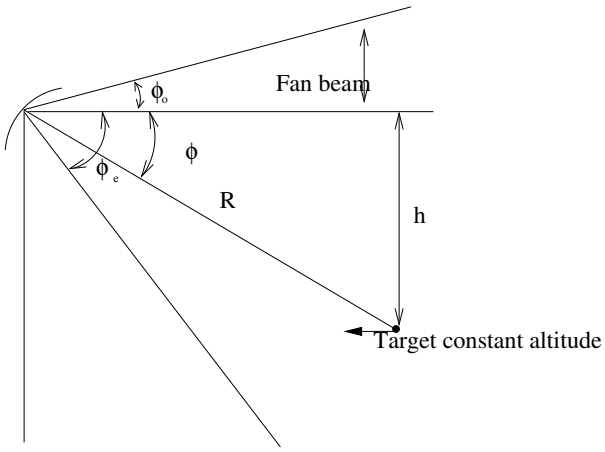

Figure 3.5: Target in Cosecant-Squared Antenna Beam.

where K_1 is given by

$$K_1 = \frac{K \times G(\phi_\circ)}{csc^4\phi_\circ}$$

From Figure 3.5,

$$sin\phi = \frac{h}{R} \tag{3.27}$$

Substituting in Equation 3.26, the received power is given by,

$$P_{rx} = \frac{K_1}{h^4} \tag{3.28}$$

Figure 3.6 shows the simulation of the cosecant-squared gain with elevation. A 3-dB elevation beamwidth of 30° and fan beam of 6° were used in the simulation. The gain drops rapidly with elevation angle such that a constant gain is achieved for targets at the same height but increasing range.

3.5 Radar Cross Section

To model the backscatter power, the type and properties of the targets need to be known. Different targets have varying reflectivity depending on their size and their orientation relative to the radar.

The *radar cross section* (RCS) describes the apparent area of the target as perceived by the radar and is a measure of how much power flux is intercepted by the target and re-radiated to the radar [6]. As a measure of the return power at the front-end of the receiver, different targets are used to simulate the ground return. The targets can be categorized into two types namely [15, pg18],

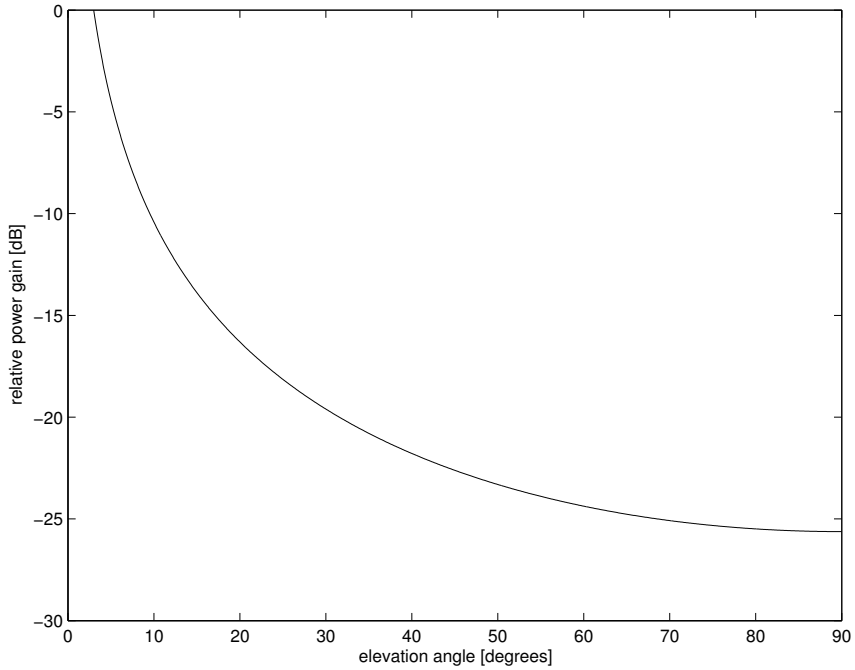

Figure 3.6: Cosecant-Squared Antenna Pattern.

1. Distributed Targets.
2. Point Targets.

The RCS of a distributed target such as a wheat field is given by,

$$\sigma_t \;=\; \sigma^{\circ}(\theta) \;\times\; A_c\,[\mathrm{m}^2] \tag{3.29}$$

where σ° is the backscatter coefficient as described in Section 2.2.4 and $A_c$represents the clutter area.

The backscattering coefficient values for the different distributed targets used in the simulation of the return power, are obtained from Ulaby [15, pg91] and are modelled statiscally by,

$$\sigma^{\circ}_{mean}(\theta) = P_1 + P_2 exp(-P_3\theta) + P_4\cos(P_5\theta + P_6) \tag{3.30}$$

where P_n is the loading parameter.

3.5.1 Distributed Targets

The distributed targets used can be classified into 4 main groups namely:

1. Barren and sparsely vegetated land.
2. Vegetated land.
3. City.
4. Sea.

Barren and sparsely vegetated

Barren land is characterised by the scarcity of vegetation and is defined as comprising of bedrock, gravel, desert pavement and soil.

Vegetated land

Vegetated land includes naturally occurring vegetation and agricultural crops and can be further sub-divided into:

- Trees and Forests such as broadleaf trees and needle-leaf evergreens.
- Shrubs and bushy plants. They include natural shrubs, large grains (corn), legumes (beans, peas), root crops.
- Grasses. These include natural rangeland, pasture, hay and small cereal grains (barley, oats and wheat).

City

Urban land is defined as extended surfaces constructed by man or areas of land dominated by man-made structures. The backscattering coefficient for city was inferred from Skolnik [7] with varying incidence angle.

3.5.2 RCS for Bandwidth-Defined Ground Strip

The instantenous return power at the antenna output gives an indication of the maximum power that the receiver is required to handle before amplification occurs. The receiver has a front end bandwidth of 200 MHz. Essentially, the time, t_r, required for the output of the waveform to rise from its minimum to its maximum is given by [8],

$$t_r = \frac{1}{B_r} \tag{3.31}$$

The stripwidth on the ground that results in the maximum return is given by [10],

$$\begin{aligned} \delta R_{gr} sin(\theta) &= \frac{ct_r}{2} \\ \delta R_{gr} &= \frac{ct_r}{2sin(\theta)} \quad (3.32) \\ &= \frac{c}{2\,B_r\,sin(\theta)} \quad (3.33) \end{aligned}$$

where θ is the incidence angle.

The factor of "$\frac{1}{2}$" comes from the fact that the pulse travels to and from the patch on the ground represented by t_r seconds. The ground clutter area, A_c, at a range, R, illuminated by an antenna with a 3-dB azimuth beamwidth, ϕ_a, shown in Figure 2.2 is given by,

$$A_c = R \times \phi_a \times \delta R_{gr}$$

The RCS, σ_t, is thus given by,

$$\sigma_t = \sigma^{\circ}(\theta) \times A_c$$

where $\sigma^{\circ}(\theta)$ is the radar backscattering coefficient at different incidence angle.

3.5.3 RCS for Point-Like Targets

Some targets have large values of RCS owing to their size and orientation and consequently, reflect a large portion of the incident power. The specific values for the RCS of such targets, obtained at X-band from [7], are used in the simulation of the maximum power return. Table 3.3 shows the values of RCS for some targets at X-band[2]. The RCS of the triangular corner reflector found at RRSG-UCT (with length 1.5m) is also included and is given in [10, pg52] as,

$$\begin{aligned} RCS &= \frac{4\pi a^4}{3\lambda^2} \quad (3.34) \\ &= 20379\,[\mathrm{m}^2] \quad (3.35) \\ &= 43.1\,[\mathrm{dBm}^2] \quad (3.36) \end{aligned}$$

[2]The RCS for the corner reflector, in Table 3.3, was worked out from actual dimensions of the one at UCT and not obtained from the same reference.

Table 3.3: RCS of specific targets at X-band (from [13, pg44])

Targets	RCS [m^2]	RCS [dB]
Bird	0.01	-20
Man	1	0
Automobile	100	20
Truck	200	23
Corner Reflector	20379	43.1
road traffic	100	20
Cabin Cruiser	10	10

3.6 Front End Power

The front-end return power at the antenna output is modelled using the following equation [10, pg6],

$$P_{rx} = \frac{P_{tx}\, G^2\, \lambda^2\, \sigma_t}{(4\pi)^3\, R^4\, L_s}[\mathrm{W}] \tag{3.37}$$

The losses in the duplexer and *transmit-receive* (TR) cell are incorporated in the "L_s" term while an antenna efficiency of 60% is assumed and included in the gain term. Different scenarios are simulated and the return power with range-dependent incidence angle is calculated. A sinc-squared antenna pattern is used in the simulations and the boresight axis of the antenna is varied in its position on the swath width. The RCS, σ_t, of the distributed targets are modelled for a clutter area, A_c, as explained in Section 3.5.2. The results of the simulations performed are shown in Subsections 3.6.2 and 3.6.1.

3.6.1 Peak Return Power Point-Like Targets

Along the swath width certain targets will appear very bright and reflect a large portion of the incident power. To cater for such targets so that they do not saturate the receiver, the received power was simulated for targets with large RCS at X-band.

For the largest power return simulation, the brightest target "seen" by the radar was assumed to be the corner reflector in the far-field of the antenna with the antenna boresight pointing on the axis of the corner reflector. Table 3.4 shows the power budget of such a target.

Table 3.4: Power Budget for Corner Reflector.

P_{tx}	65.44	[dBm]
G^2	49.4	[dB]
λ^2	-29.8	[dBm^2]
σ_t	43.1	[dBm^2]
$(4\pi)^3$	-33	[dB]
R^4	-139	[dBm^4]
L_s	-10	[dB]
P_{rx}	-53.86	[dBm]

Other man-made targets that will behave like bright point targets, have also been included in the simulation of return power as shown in Figure 3.7. The antenna is assumed to have 3-dB elevation beamwidth of 30° and a 3-dB azimuth beamwidth of 3°.

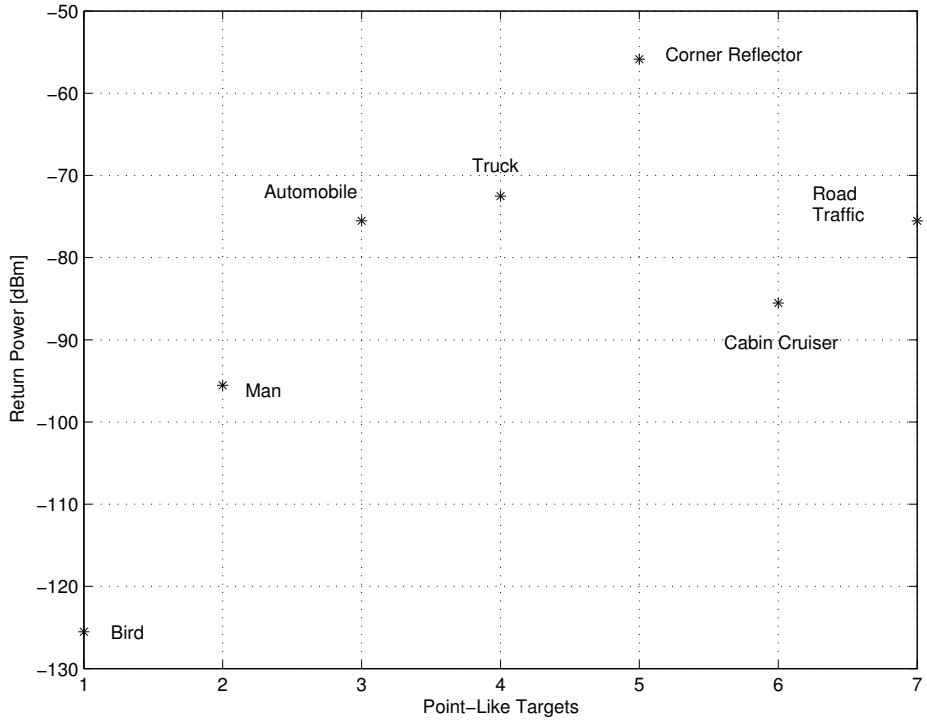

Figure 3.7: Peak Power Return of Point-Like Targets at X-Band.

3.6.2 Peak Return Power for Distributed Targets

The peak power received from the distributed targets, allows one to design the subsequent receiver stages, such that the components are not driven into saturation and hence, produc-

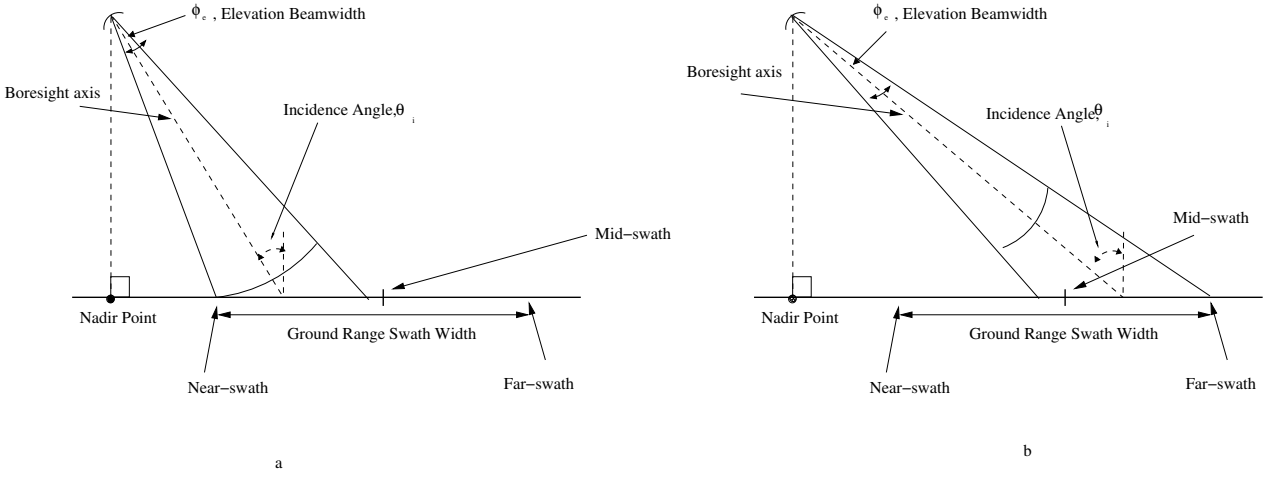

Figure 3.8: Boresight Axis Position on Swath Width

ing unwanted harmonics. The front-end power return at the antenna output is simulated for 8192 range bins, using models of the different distributed targets, and the antenna boresight is pointed to various points on the swath width, namely:

- The near-swath.
- The mid-swath.
- The far-swath.

The backscattered power is simulated for the front-end of the receiver and hence the uncompressed pulse length is used in calculations. This pulse length, τ, corresponds to the inverse of the -3-dB bandwidth of the front-end of the receiver, which is 200 MHz, as explained in Section 3.5.2.

Figures 3.8a and 3.8b show the antenna position on the swath width for the near-swath and the far-swath setup respectively.

The $\ddot{}\frac{1}{R^4}\ddot{}$ term, in Equation 3.37, is responsible in attenuating the backscattered power for targets at far range. By placing the boresight axis of the antenna at different position on the swath width, the attenuating effect of the targets at long range is partly compensated by the increase in gain due to the targets falling in the 3-dB beamwidth of the antenna. The results of the power return simulations are shown in the figures below.

Figure 3.9 shows the return power at the antenna output versus the ground range from the nadir point. The near-incidence angle is 40° and the antenna boresight close to the near-swath. The increase in the power level in the near-swath and the short range contribute in boosting the power received for targets falling in the 3-dB beamwidth of the antenna.

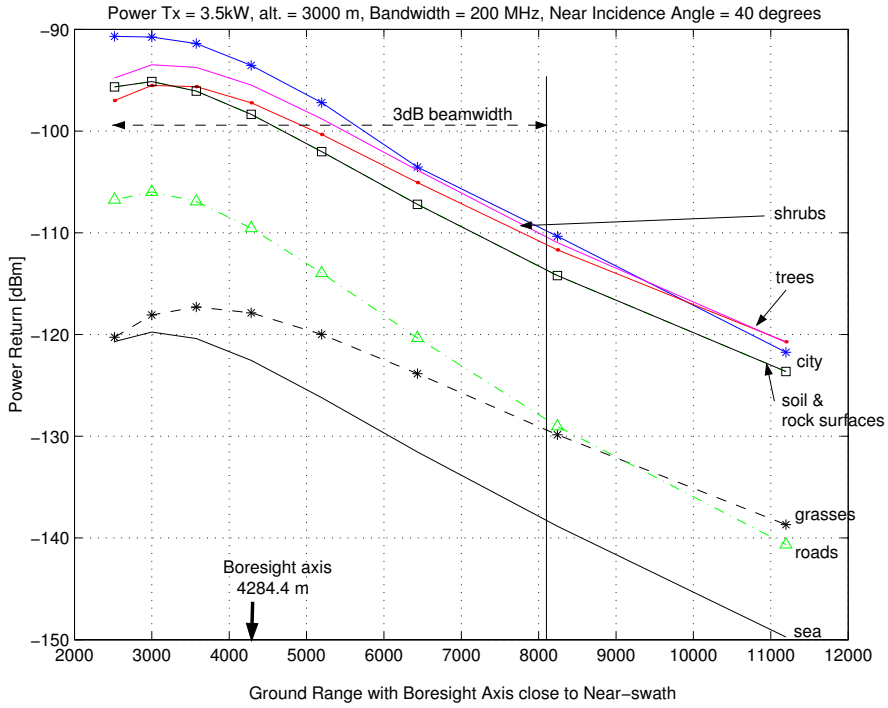

Figure 3.9: Peak Power Return with Boresight Axis Close To Near-Swath.

Figure 3.10 shows the variation of front-end power return at the antenna output with the boresight of the antenna on the swath centre. Compared to Figure 3.9, the received power is relatively flat for the far-incidence angle while the initial drop for the near-incidence angle is a result of targets falling outside the 3-dB beamwidth of the antenna.

Figure 3.11 shows the variation of the front-end power return with the boresight of the antenna close to the far-swath. This has a considerable advantage in boosting the far-swath power return. Targets such as trees have their backscattered power increased by approximately 7 dB, from -121 dBm to -113 dBm, with the radar in such a configuration as opposed to having the boresight axis closer to the near-swath.

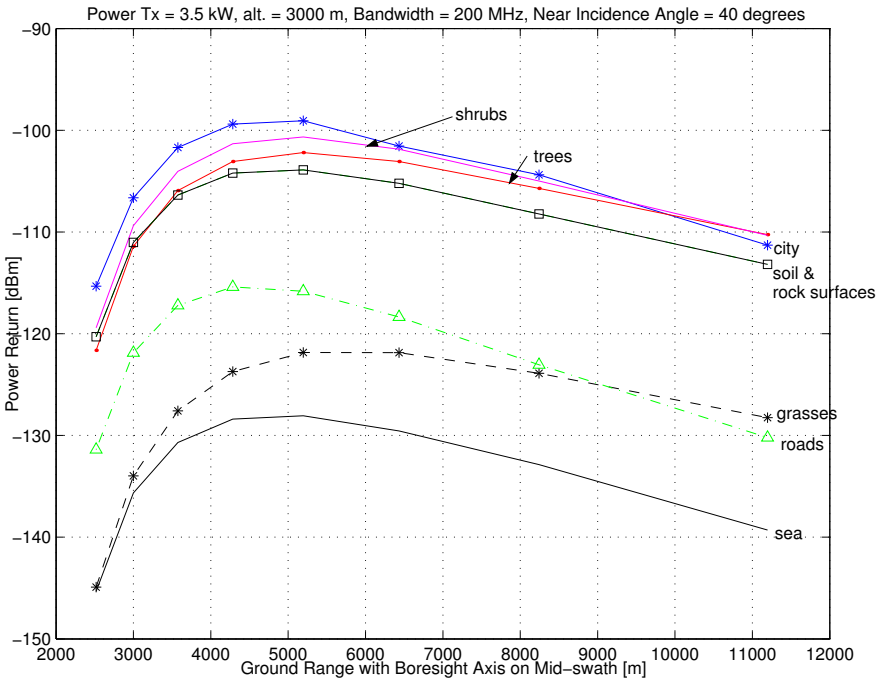

Figure 3.10: Peak Power Return With Boresight Axis On Swath Centre.

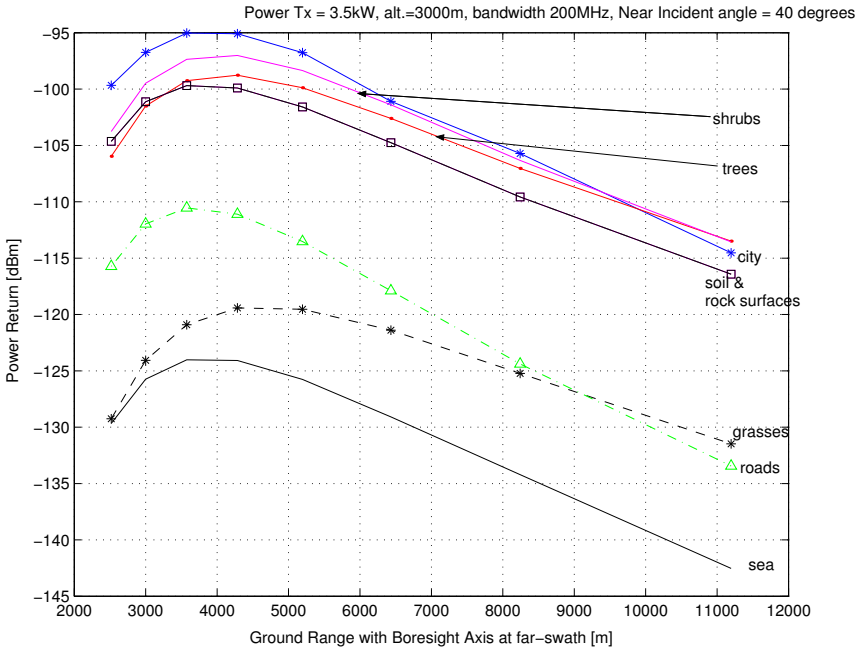

Figure 3.11: Peak Power Return With Boresight Axis Close To Far-Swath.

Chapter 4

The Receiver Design

4.1 Introduction

The receiver output has to be fed into the *analogue-to-digital converter* (ADC) for digitisation and the appropriate power level is required. Noise limits the smallest detectable signal while the largest signal is limited by distortions arising from nonlinearity of the receiver components. The receiver is made up of filters, mixers and gain blocks. A preliminary receiver is shown in Figure 4.1 with the two downconversion stages, *sensitivity time control* (STC) and *manual gain control* (MGC). This chapter describes the implementation of an optimised receiver from parameters obtained from Chapter 3. Section 4.2 treats noise and cascaded noise figure. The choice of the operating frequency is described in Section 4.3. The use of the *low noise amplifier* (LNA) is explained in Section 4.4 while Section 4.5 deals with the choice of the RF filter and its use in minimising noise input in the receiver. The mixers chosen is described in Section 4.6 with an explanation of the factors affecting their performance. The IF stages, namely the STC and MGC, are treated in Sections 4.7 and 4.8 respectively. Section 4.10 shows the actual detailed receiver design. The receiver level table and diagram that were used in implementing the receiver, is detailed in Section 4.11.

4.2 Noise

The receiver encounters two types of thermal noise namely:

- Noise captured by an antenna facing a blackbody (which is assumed to be at a physical temperature of 290 K).
- Noise generated by the components in the receiver.

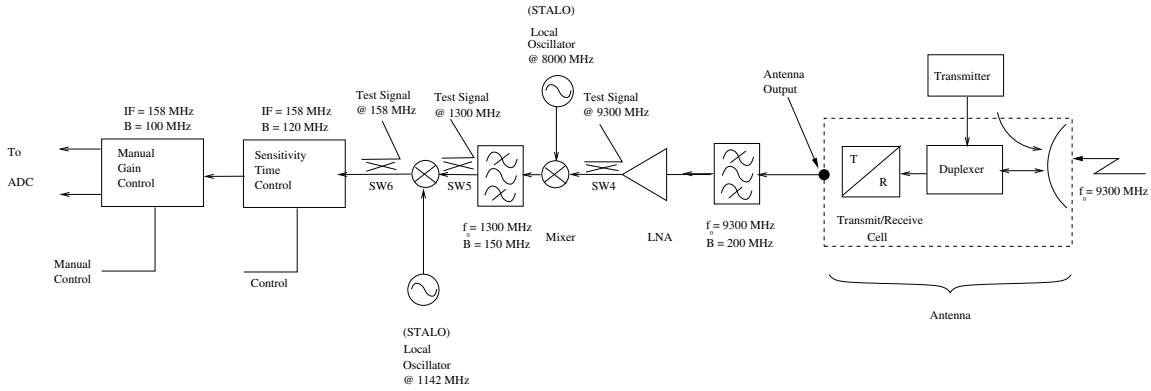

Figure 4.1: Radar Receiver Block Diagram.

The noise power at the antenna output is given by [14, pg52],

$$\begin{aligned} N &= kT_{\circ}B && (4.1)\\ &= 1.38 \times 10^{-23} \times 290 \times 200 \times 10^{6}\,[\mathrm{W}] && (4.2)\\ &= -90.97\,[\mathrm{dBm}] && (4.3) \end{aligned}$$

The noise needs to be tracked down the receiver such the signal-to-noise ratio is known at the ADC.

4.2.1 Noise Figure

The noise figure of a system is a figure of merit specifying how noisy a component or a system is, measured in decibel[6, 14]. The noise figure is measured over the linear part of the operating range of the system and is given by,

$$F = \frac{(SNR)_i}{(SNR)_o} \tag{4.4}$$

The noise figure leads to a concise way of specifying the noise temperature of the components in the receiver. Figure 4.2 below shows the equivalent circuit of the receiver. The noise input to the receiver is given by,

$$N_i = kT_oB \tag{4.5}$$

where B is the noise bandwidth.

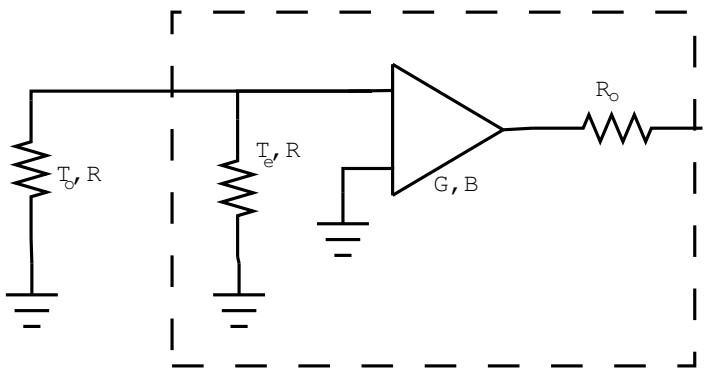

Figure 4.2: Receiver Equivalent Circuit.

The thermal noise added by the receiver is represented by an equivalent noise temperature, T_e, referred to the amplifier input. The total output noise is thus given by,

$$N_o = (N_i + k\,T_e\,B)\,G \tag{4.6}$$

The noise figure is related to the equivalent noise temperature, T_e, and is given by [8, pg200],

$$F = 1 + \frac{T_e}{T_o} \tag{4.7}$$

For calculations of the noise temperature, the single sideband noise figure was used as the image signal contributes no information but only noise.

4.2.2 Cascaded Noise Figure

The receiver is essentially a cascaded system with *n* components, each having its own properties in terms of gain, bandwidth, losses and noise figure. Figure 4.3 shows the cascaded blocks in a receiver. Each component is tagged with its gain, G, noise figure, F and bandwidth, B_r.

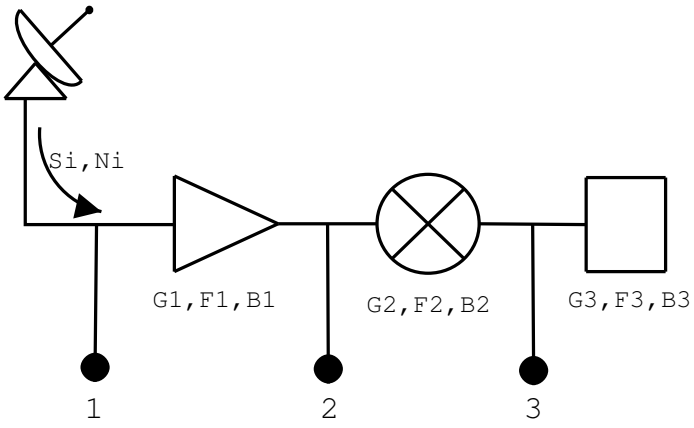

Figure 4.3: Cascaded Circuit Diagram.

The overall noise figure of the system is given as [14, pg155],

$$F = F_1 + \frac{F_2 - 1}{G_1} + \frac{F_3 - 1}{G_1 G_2} + ... + \frac{F_n - 1}{G_1 G_2 ... G_{n-1}} \tag{4.8}$$

4.3 Operating Frequency

4.3.1 Carrier Frequency

The *intermediate frequency* (IF) has been chosen to be 158 MHz after considering the sampling rate of the ADC. The maximum sample rate of 210 MHz was assumed in the design of the 2^{nd} band of aliasing. With a bandwidth of 100 MHz, the 2^{nd} band of aliasing has centre frequency of 157.5 MHz with the 2.5 MHz margin band as shown in Figure 4.4. The choice of 158 MHz results from the preference of an integer value for generating the local oscillator. In view of the TWTA (travelling wave tube amplifier) available, the carrier frequency has been set to 9300 MHz.

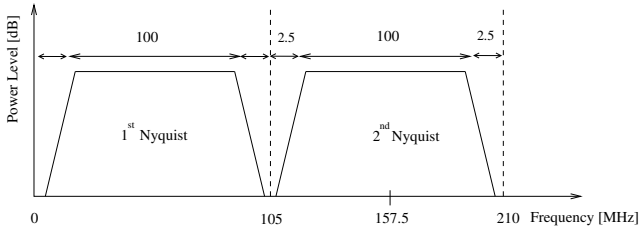

Figure 4.4: 2^{nd} Nyquist Spectrum.

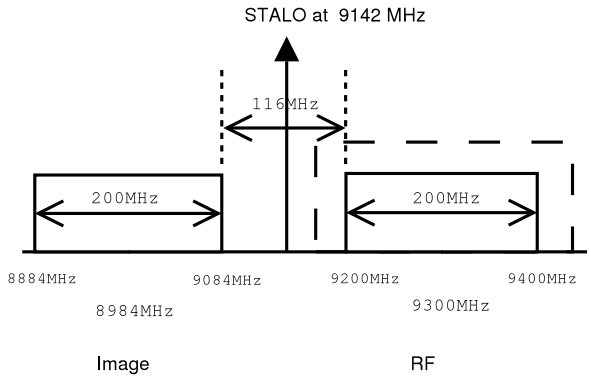

Figure 4.5: Single Stage Downconversion.

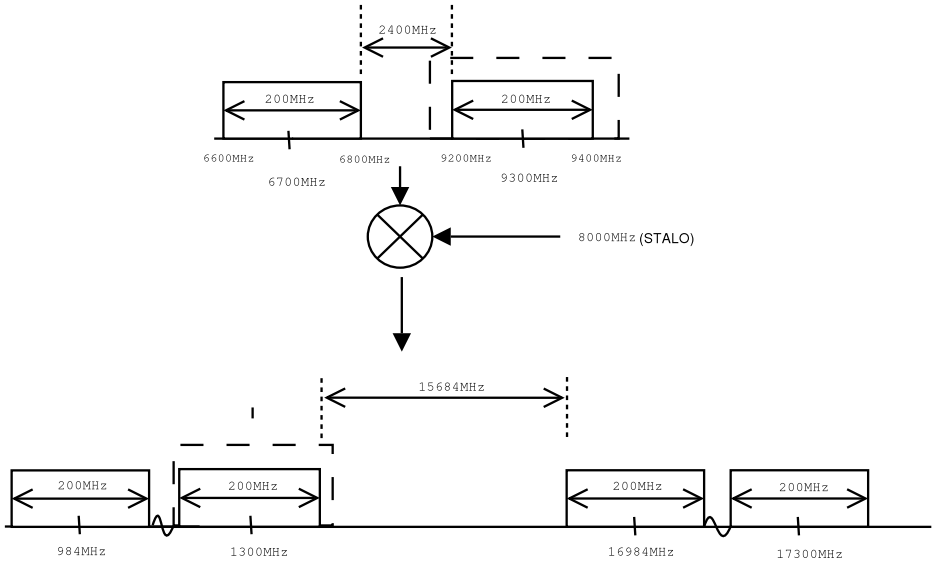

Figure 4.6: Dual-stage Downconversion.

4.3.2 Stable Local Oscillator (STALO)

A two-stage downconversion has been chosen to bypass the need for a sharp cut-off since the image frequency will be centred at 8984 MHz as shown in Figure 4.5 for a single downconversion to 158 MHz and the separation being 116 MHz.

Using a dual-stage downconversion, from the *radio frequency* (RF) centred at 9300 MHz, a first downconversion stage at L-band is used followed by a second downconversion to the required IF of 158 MHz. Figure 4.6 shows a schematic of the different downconversion stages and the frequency spread which is improved from 116 MHz to 2400 MHz with the image frequency in the dual stage shifted to 6700 MHz.

4.4 Low Noise Amplifier

An RF amplifier is a network device that increases the amplitude of a weak signal, thereby allowing further processing by the receiver. Being the first gain stage in the receiver, it also sets the noise property of the system as can be inferred from Equation 4.8. Hence, an LNA with high gain and low noise figure is chosen as the first stage RF amplifier. The choice of 22 dB gain and 0.9 dB noise figure of the LNA, results in a high gain in the RF stage but low enough such that the receiver is not driven into compression in the later stages.

4.5 RF Filter

An RF filter is used to allow a range of desired frequencies to pass through the network and attenuating signals outside the passband. A 5^{th} order butterworth filter is used in the receiver chain to reject frequencies outside the passband and to limit the noise going through the receiver chain. It offers a flat passband and a phase response that is nonlinear about the cut-off frequency with a group delay that increases slightly towards the band edges. A compromise has to be made to ensure low ripple and low phase distortions, hence the use of a Butterworth filter design. A preselect filter of 200 MHz bandwidth is used to prevent signals from outside the passband from saturating the LNA and to limit the noise input.

4.6 Mixers

Mixers are used to translate an RF frequency from a high level to a lower IF in the receiver stage. The mixer design uses nonlinear devices, e.g. diodes or transistors, because nonlinearity is required for the production of frequencies not present at the input [19]. Figure 4.7 shows a mixer driven by a stable LO signal and its output.

The RF and stable LO frequencies are spaced apart by an amount equal to the IF. The downconversion signal is the difference between the RF and LO frequency. The image frequency has the opportunity to mix with the LO for an IF response and care must be taken to attenuate this signal and provide protection. The preselect filter and a dual-conversion stage receiver design provides separation and rejection of the image signal. A double-balanced mixer is used for both the 3^{rd} and 2^{nd} downconversion stage, as it offers advantages in third order intermodulation distortion performance compared to single-ended mixer because of the balanced configuration and isolation of the RF and LO [19].

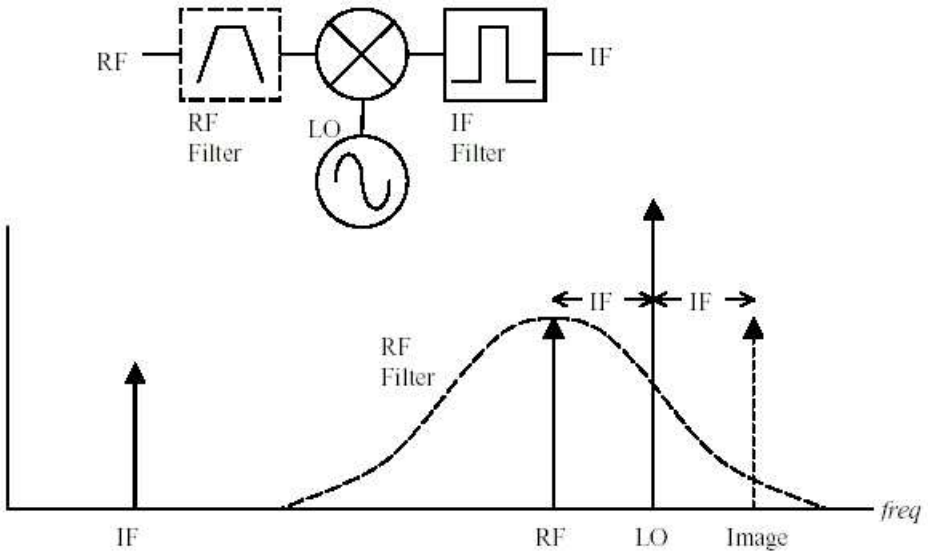

Figure 4.7: RF and Image Output from a Mixer [18].

4.6.1 Conversion Loss

While mixers operate in the linear region of the diodes or transistors, an increase in IF power relates to an increase in the RF power. With a diode mixer, the mixer is passive and has a conversion loss. Figure 4.8 shows the 1 dB point which is where the the power output is 1 dB lower than the output power of the linear region. Care must taken not to drive the mixers near their 1 dB compression point or else the loss in output power will increase and harmonics and intermodulation components will be generated.

$$\text{Conversion loss} = 10 \lg \frac{\mathrm{P}_{RF}}{\mathrm{P}_{IF}} [\mathrm{dB}] \tag{4.9}$$

4.6.2 Intermodulation Reduction

Intermodulation products are produced when two or more signals at frequencies f_1 and f_2 are applied to a nonlinear device [14]. These may be the second-order $f_1 \pm f_2$ products, third-order $2f_1 \pm f_2$, $2f_2 \pm f_1$ products and so on.

The two-tone third-order products are given by,

$$\begin{aligned} f_{IM1} &= (2f_1 - f_2) - f_{LO} \\ &= (2f_2 - f_1) - f_{LO} \end{aligned} \tag{4.10}$$

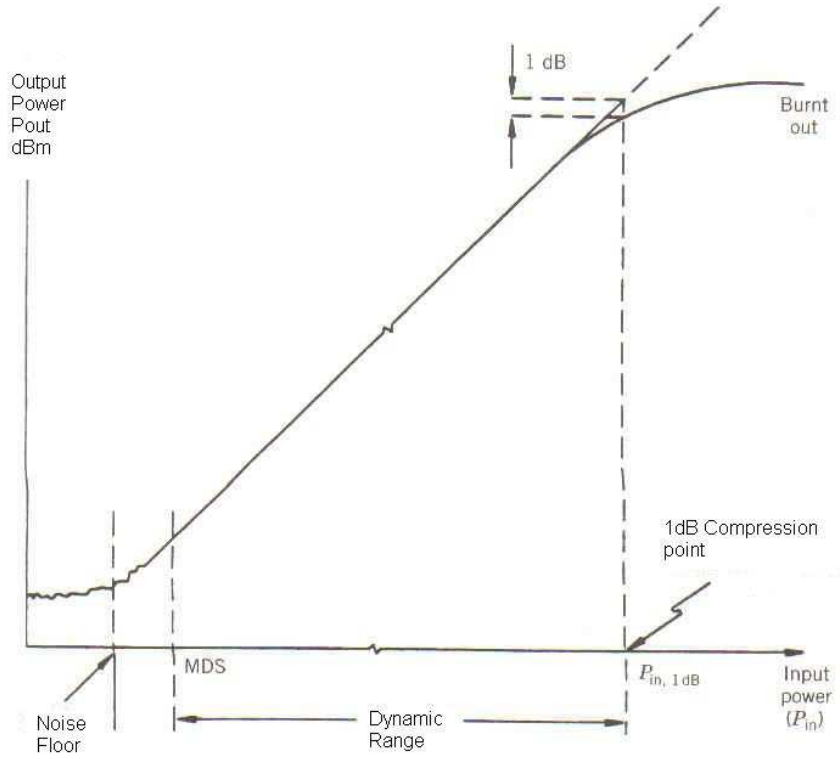

Figure 4.8: 1-dB compression point [14].

A high intercept point is required since it means high suppression of undesired intermodulation products. The *third-order intercept* (TOI) point is a theoretical point where the desired signal and the third-order distortion have equal magnitudes as shown in Figure 4.9.

Figures 4.10 and 4.11 shows the output power level of the intermodulation products of the two mixers used as per their data sheet relative to the IF output.

4.7 IF Filter

The IF filters have been chosen to be of the same order as the RF filter. Essentially, 5^{th} order butterworth filters are used in all the downconversion stages with the 3-dB bandwidth closing up from 200 MHz to reach 100 MHz, at the input of the ADC.

Figure 4.12 shows the theoretical filter transfer function of the receiver with the image frequency of 6700 MHz at -19.3 dB relative to the RF and the attenuation of unwanted signals as they go down from the 3^{rd} downconversion stage through to the 1^{st} stage. The fall-off rate for an n^{th} order butterworth filter is 6n dB/octave [20, pg268]. Image frequencies, RF and LO frequencies are shown with their attenuation relative to the centre

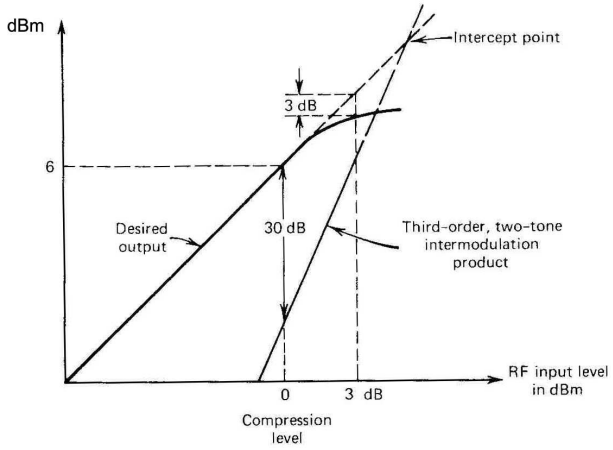

Figure 4.9: Third Order Intercept Point [14].

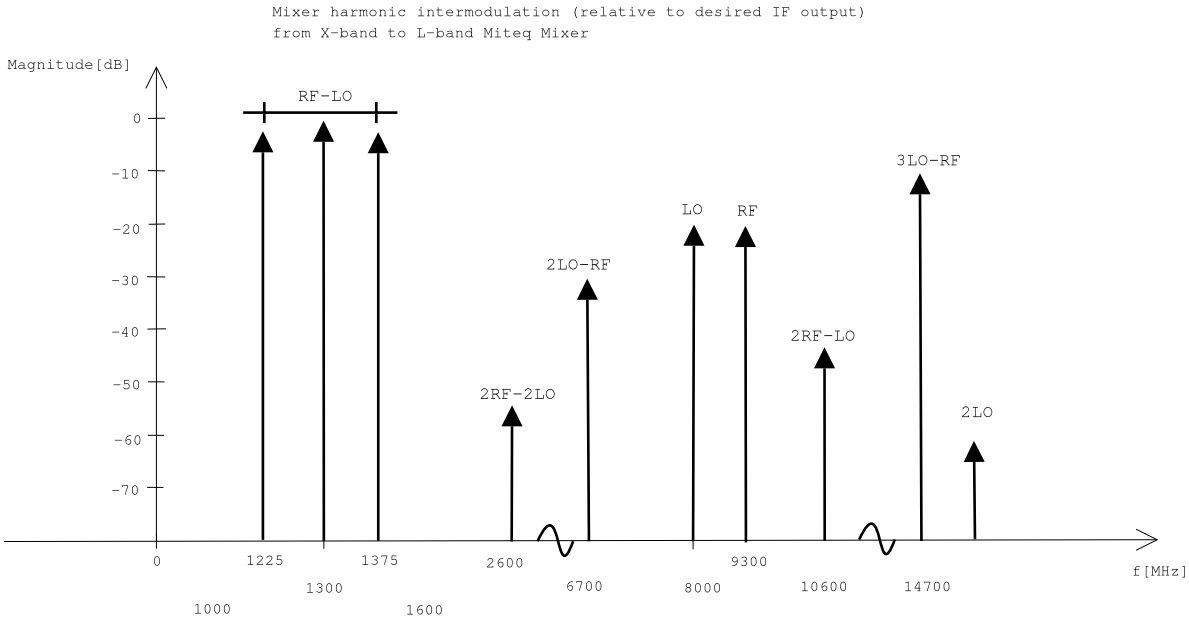

Figure 4.10: Spurious Reponse Levels at the X-band to L-band mixer.

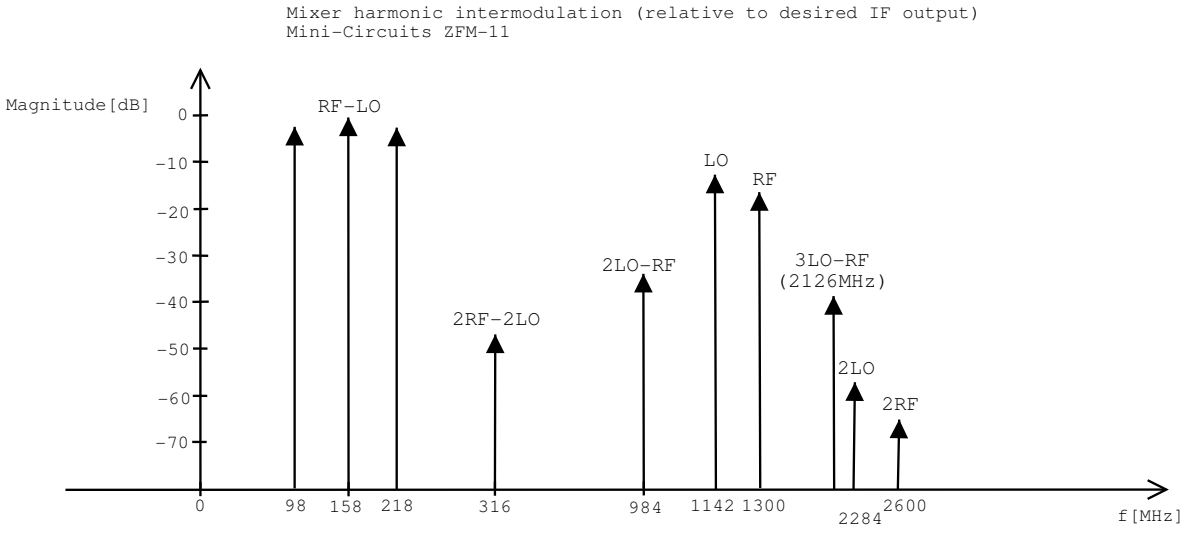

Figure 4.11: Spurious Response Levels at the Mixer Output for the 1st Downconversion Stage.

IF.

4.8 Attenuation and Gain

The 1st IF is divided into two parts namely the *sensitivity time control* (STC) and *manual gain control* (MGC). Power return from different targets may have widely varying amplitudes such that the dynamic range of the receiver may be exceeded. This will put a constraint on the ADC stage where power return from some targets at far range may be outside the dynamic range of the ADC and therefore such targets will not be resolve by the ADC.

4.8.1 Sensitivity Time Control

The STC is a variable gain stage with time, where the amplitudes of the echoes from targets at far range are boosted. To achieve a fairly constant power return with time, the STC must have at a variable gain of up to 20 dB. Figure 4.13 shows the variation of gain with ground range (which is related to time) for the different terrains modelled. This STC curve has to be preloaded in the receiver controller board. This is implemented in the receiver using an electronic attenuator which has an attenuation that varies with an applied control current.

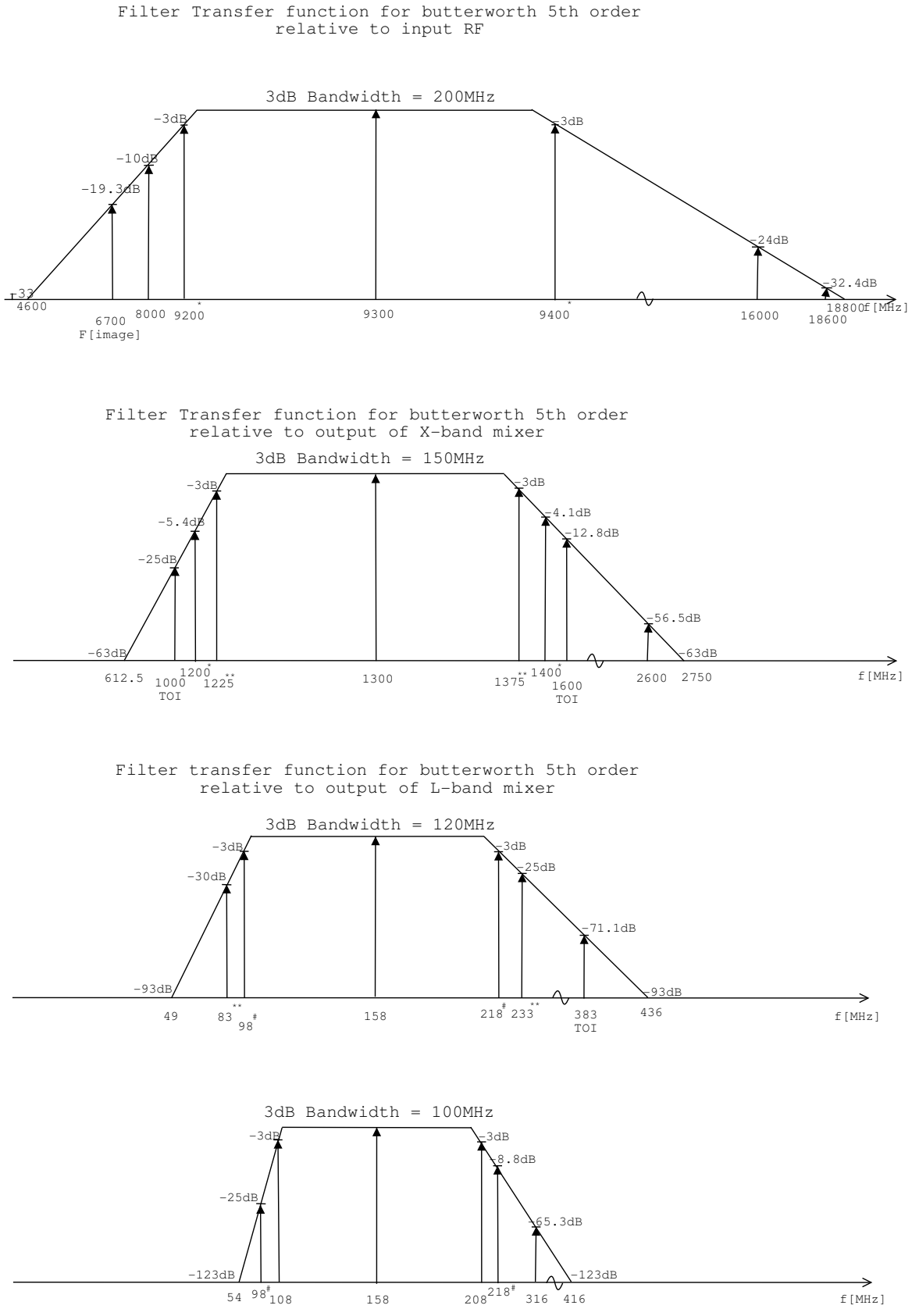

Figure 4.12: Filter Transfer Function.

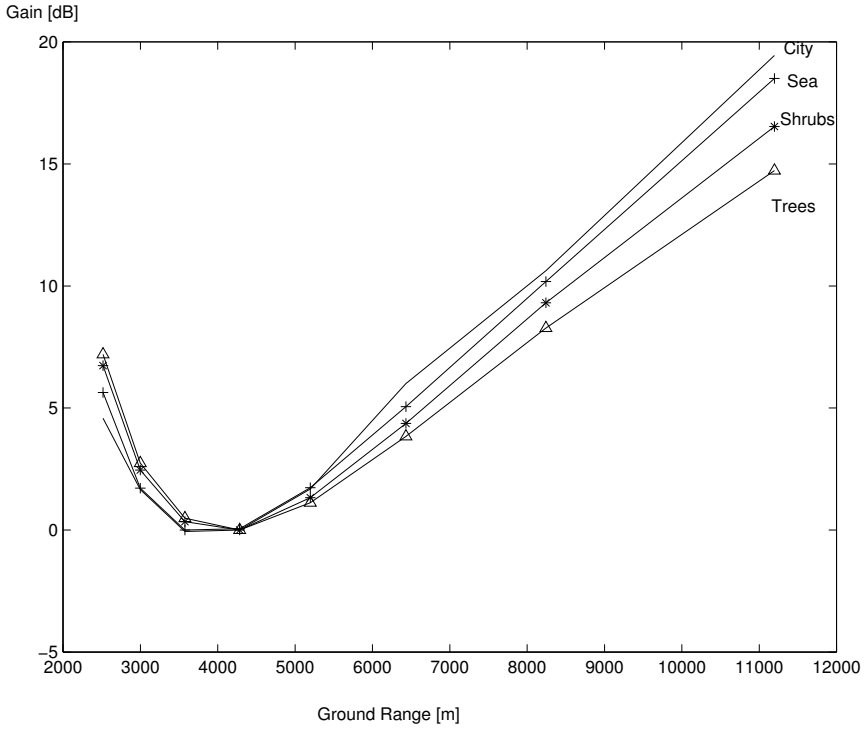

Figure 4.13: STC Curve with Ground Range.

4.8.2 Manual Gain Control

The MGC consists of a 3-bit digital attenuator followed by gain blocks. Owing to the fact that corner-reflector-type targets will not be significant when flying the SAR over certain distributed targets like wheat field or forest, the MGC is used to boost the gain thereby improving the noise figure. When flying over city or other terrains where large targets, are expected to dominate, the MGC is switched on to limit the power in the receiver and hence avoiding the receiver from being driven into compression. An attenuator of 30 dB dynamic range is used to attenuate the input from large targets.

4.9 Switches

As an integral part of the transceiver test loops have been included in the design of the receiver. The *single pole double throw* (SPDT) switches are chosen to cater for power and centre frequency of the different IF. The SPDT switches are to be connected to the transmitter such that each of the three IF stages can be tested at a time in the laboratory.

4.10 The SAR Receiver

Figure 4.14 shows the receiver as it has been designed with the constraints taken into consideration. The components are built in modules and connected via SMA male-ended coaxial connectors and were chosen according to the specifications in their respective data sheets. The LNA is connected to the waveguide filter using a barrel connector to reduce cable length and improving the noise figure. The components are referred to, by the acronyms given, in the subsequent chapters of this dissertation.

4.11 Budget Analysis

The receiver budget analysis and hence, the receiver level diagram allows, in an easy way, the tracking of the signal peak along the cascaded blocks in order to prevent the saturation of the amplifiers, thus producing harmonics.

From Figure 4.3, the noise level at each node can be calculated using Equations 4.5, 4.6, 4.7.

At node 1,

$$N_i = kT_0B_r \tag{4.11}$$

where B_r is the bandwidth of the bandpass filter prior to the LNA.

At node 2,

$$N_{o2} = (kT_oB + kT_eB_1) \times G_1 \tag{4.12}$$

where $T_e = (F_1 - 1)T_o$ giving,

$$N_{o2} = kT_oG_1 \left(B + (F_1 - 1)\, B_1\right) \tag{4.13}$$

where B_1 is the operating bandwidth of the amplifier.

Thus, given the noise figure of each component and the operating bandwidth, the noise output after each component can be calculated. Table 4.1 shows the values obtained, in simulations of the peak power, for a corner reflector, noise level input and the cumulative noise figure of the system. A theoretical noise figure of 2.47 dB is expected from the design of the receiver with minimum attenuation. The worst-case noise figure is calculated to be 7.96 dB as can be inferred from the cumulative noise figure at the splitter SP2 output from Table 4.2.

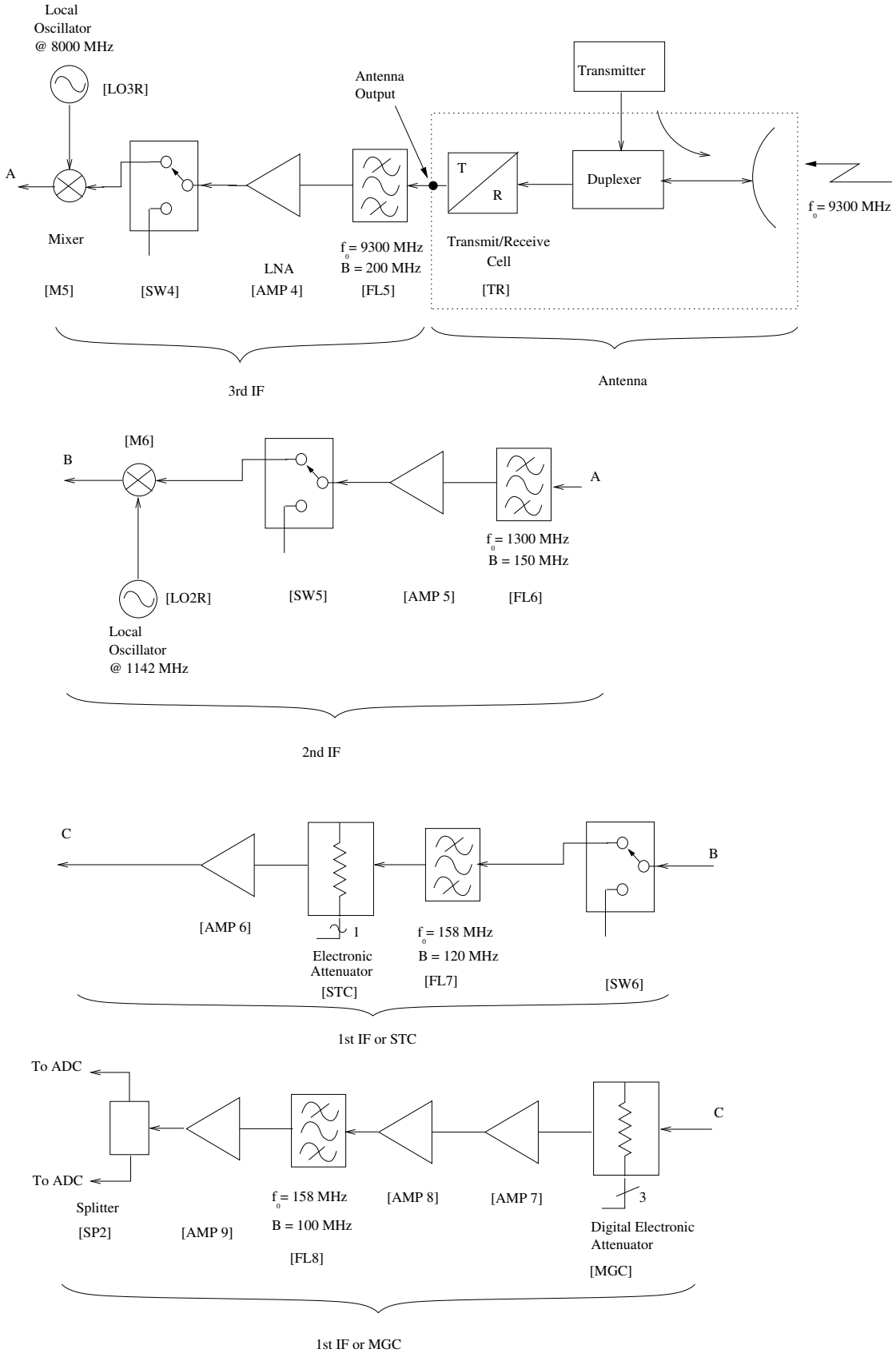

Figure 4.14: The SAR Receiver

Table 4.1: System Budget Calculations For Minimum MGC Attenuation.

Components	Input	FL5	LNA	SW4	M5	FL6	AMP5	M6	FL7	STC	AMP6	MGC	AMP7	AMP8	AMP9	FL8/SP2
Stages	1	2	3	4	5	6	7	8	9	10	11	12	13	14	15	16
Bandwidth [MHz]		200	900	18000	500	150	5000	4300	120	2000	500	1000	500	500	500	100
Noise Figure [dB]		1	0.9	1.5	6	1	1.5	7	1.2	20	3.8	5	3.8	3.8	3.8	4
Gain [dB]		-1	22	-1.5	-6	-1	28	-7	-1.2	-20	20	-5	20	20	20	-4
Cumulative Gain [dB]		-1	21	19.5	15	14	42	35	33.8	13.8	33.8	28.8	48.8	68.8	88.8	84.8
Signal (max) [dBm]	-50	-48.74	-26.74	-28.24	-32.74	-33.74	-5.74	-12.74	-13.94	-33.94	-13.94	-18.94	1.06	21.06	41.06	37.06
Noise [dBm]	-90.97	-90.97	-65.88	-67.29	-71.78	-72.76	-44.501	-51.49	-52.49	-72.09	-51.90	-56.90	-36.89	-16.89	3.11	-0.89
1 dB compression pt. [dBm]			8		-1		10				16		16	16	16	
Cum. Noise Figure [dB]			1.9	1.91	2.00	2.03	2.10	2.10	2.10	2.25	2.46	2.46	2.47	2.47	2.47	2.47

Table 4.2: System Budget Calculations For Maximum MGC Attenuation.

Components	Input	FL5	LNA	SW4	M5	FL6	AMP5	M6	FL7	STC	AMP6	MGC	AMP7	AMP8	AMP9	FL8/SP2
Stages	1	2	3	4	5	6	7	8	9	10	11	12	13	14	15	16
Bandwidth [MHz]		200	900	18000	500	150	5000	4300	120	2000	500	1000	500	500	500	100
Noise Figure [dB]		1	0.9	1.5	6	1	1.5	7	1.2	20	3.8	35	3.8	3.8	3.8	4
Gain [dB]		-1	22	-1.5	-6	-1	28	-7	-1.2	-20	20	-35	20	20	20	-4
Cumulative Gain [dB]		-1	21	19.5	15	14	42	35	33.8	13.8	33.8	-1.2	18.8	38.8	58.8	54.8
Signal (max) [dBm]	-50	-48.74	-26.74	-28.24	-32.74	-33.74	-5.74	-12.74	-13.94	-33.94	-13.94	-48.94	-29.94	-8.94	11.06	7.06
Noise [dBm]	-90.97	-90.97	-65.88	-67.29	-71.78	-72.76	-44.501	-51.49	-52.49	-72.09	-51.90	-82.19	-60.53	-40.52	-20.52	-24.52
1 dB compression pt. [dBm]			8		-1		10				16		16	16	16	
Cum. Noise Figure [dB]			1.9	1.91	2.00	2.03	2.10	2.10	2.10	2.25	2.46	5.59	7.94	7.96	7.96	7.96

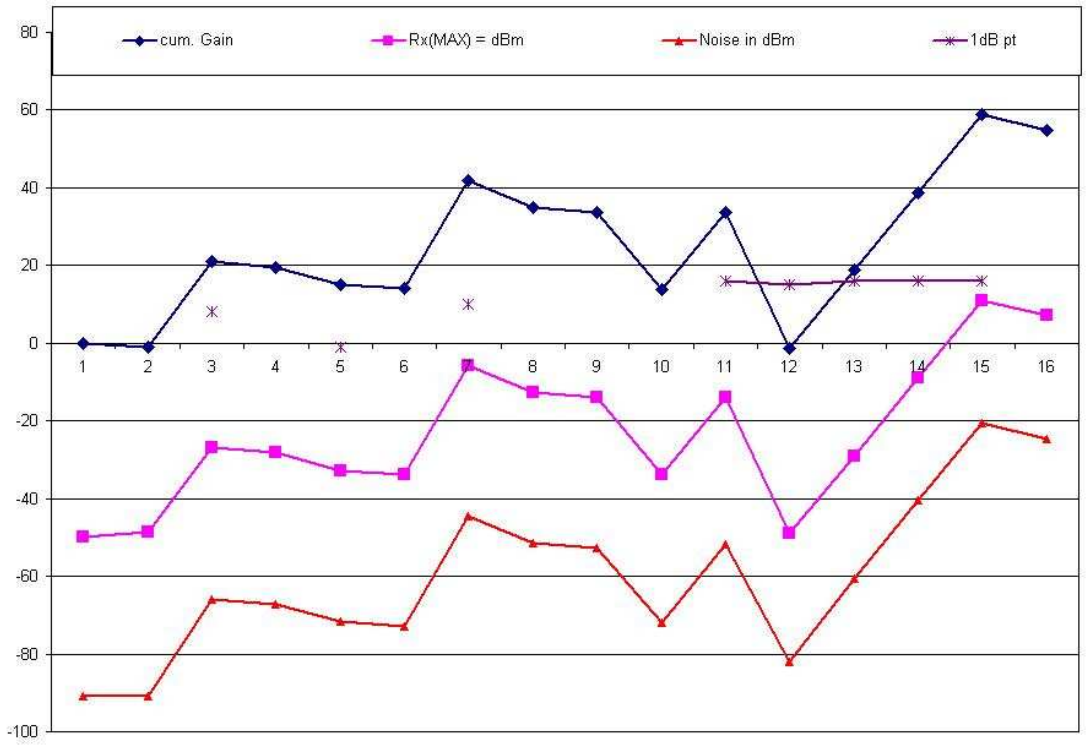

Figure 4.15: Receiver Level Diagram of Signal and Noise.

Table 4.2 is used to plot the receiver level diagram. Figure 4.15 shows the behaviour of the signal and noise from the front-end of the receiver up to the input of the ADC for a large target, e.g. corner reflector, with the front-end noise tracked up to the input of the ADC. The power levels were monitored such that they remain 2 dBm or more below the compression point.

The signal and noise levels are calculated after each component. An ADC maximum input peak power, terminated in 50 ohms, of 13 dBm was assumed. Hence, the amplification of the maximum input signal to the receiver was limited to the maximum operating input power of the ADC.

4.11.1 Resolution

Using a receiver gain of 60 dB the maximum power input at the ADC is 11 dBm. The noise input at the ADC is $-90.97 + 60 = -30.97$ dBm. In order to do signal averaging in the post processing, the *least significant bit* (LSB) of the ADC is assigned to the noise level. This results in an ADC with the following requirements,

$$
\begin{aligned}
\text{max input voltage} &= \sqrt{\frac{10^{1.1}}{1000} \times 50} \\
&= 0.7934\,[\text{V}] \\
\text{noise voltage} &= \sqrt{\frac{10^{-3.097}}{1000} \times 50} \\
&\approx 0.0063239\,[\text{V}] \\
\text{No of level} &= \frac{0.7934 - 0.0063239}{0.0063239} \\
&= 124.45 \\
&\approx 125 \\
\text{Minimum number of bits} &= \frac{log_{10}125}{log_{10}2} \\
&= 6.97 \\
&\approx 7\,[\text{bits}]
\end{aligned}
$$

4.11.2 ADC Power Calculations

Assuming an 8-bit ADC, the quantisation level is given by,

$$
\begin{aligned}
V_q &= \frac{V_{pp}}{2^n} \\
&= \frac{2}{2^8} \\
&= 7.8125\,[\text{mV}]
\end{aligned}
\tag{4.14}
$$

where n is the number of bits.

The *root-mean-square* (RMS) quantization noise power for the 8-bits ADC with $50\,\Omega$ termination is given by [8],

$$
\begin{aligned}
P_{qnt,pk} &= 30 + 10\lg\left(\frac{\frac{V_q^2}{12}}{50}\right) \\
&= -39.926\,[\text{dBm}]
\end{aligned}
$$

4.12 Summary

This chapter describes the design of the receiver to acheive a workable receiver. The thermal noise at the input of the receiver is tracked up to the input of the ADC. The

backscattered power that the receiver sees is also simulated for a known transmitted power and the receiver level diagram is used to ensure that none of the receiver components are driven into saturation. A summary of the design is described below:

- The series of cascaded filters are used to limit the noise that propagates through the receiver and are designed with a front-end -3-dB bandwidth of 200 MHZ and a last stage at the ADC input with a -3-dB bandwidth of 100 MHz.
- The receiver incorporates switches in the 3 IF stages to allow for *Built-in Test* (BIT) capabilities for preflight tests of the receiver at different IFs.
- The theoretical noise figure is calculated for the best-case to be 2.47 dB at minimum attenuation and for the worst-case to be 7.96 dB at maximum attenuation.
- The quantisation noise is designed to be at least 9 dB below thermal noise level for an 8-bit ADC. The LSB is approximately set to the noise level such that signal averaging can be performed in post processing.

Chapter 5

Receiver Tests and Results

5.1 Introduction

The receiver is divided into 3 main sections namely:

1. The 1^{st} IF.
2. The 2^{nd} IF.
3. The 3^{rd} IF.

where the 1^{st} IF is further subdivided into the *manual gain control* (MGC) section and *sensitivity time control* (STC) section as shown in Figure 5.1.

Component-level testings are performed on the different sections to verify the design of the receiver. A list of the equipment used is given below:

DC Power Supply	–	Triple Output Escort EPS-3250
	–	Triple Output HP E3630A
Spectrum Analyser	–	Agilent 9kHz - 26.5 GHz E4470B (Amplitude$\pm$0.54dB)
Sweep Oscillator	–	HP 8350B
Digital Multimeter	–	Escort EDM-2116
Power Meter	–	HP 435A ($\pm$ 1% of Full Scale)
Automatic Noise Meter	–	Agilent N8975A
Barrel Attenuator [29]	–	0 - 6 dB ($\pm$0.3 dB)
		7 - 20 dB ($\pm$0.5 dB)
		21 - 30 dB ($\pm$0.75 dB)

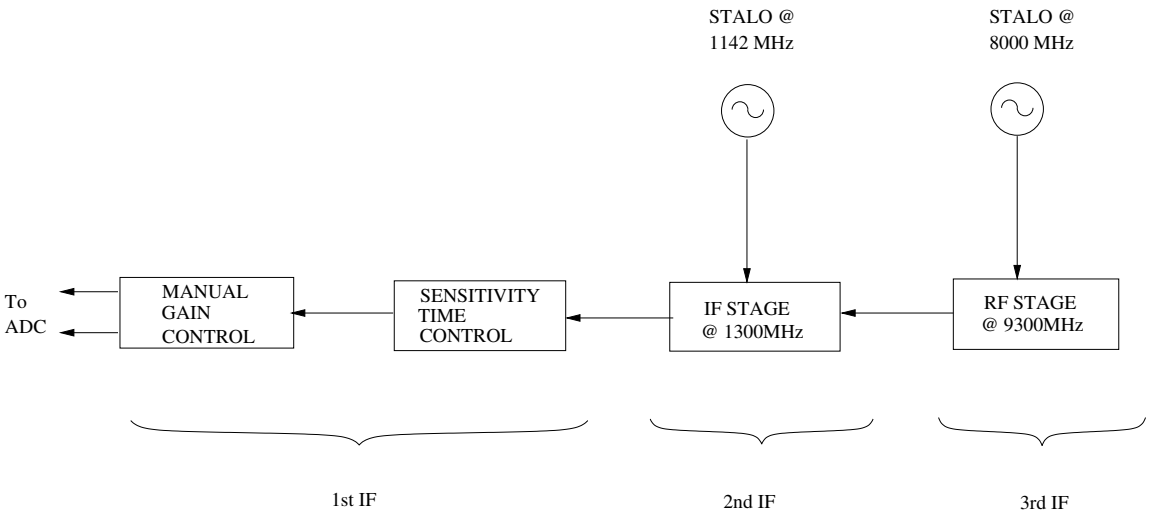

Figure 5.1: Sections of the Receiver

5.2 Amplifier Gain Test

5.2.1 1^{st} IF Amplifiers Test

The four amplifiers used in the 1^{st} IF are similar and Table 5.1 shows their properties obtained from the datasheet [28]. Tests need to be carried out to measure the gain of the amplifiers and ascertain whether they are up to specifications.

Table 5.1: Properties of ZFL-500HLN

Noise Figure [dB]	Min. Gain [dB]	DC Voltage [V]	Current [mA]	1 dB pt [dBm]
3.8	19	+15	110	+16

Equipment Required:

Sweep Oscillator, DC power supply, INMET barrel attenuators, Power Meter, Digital Multimeter, Test Cables.

Test:

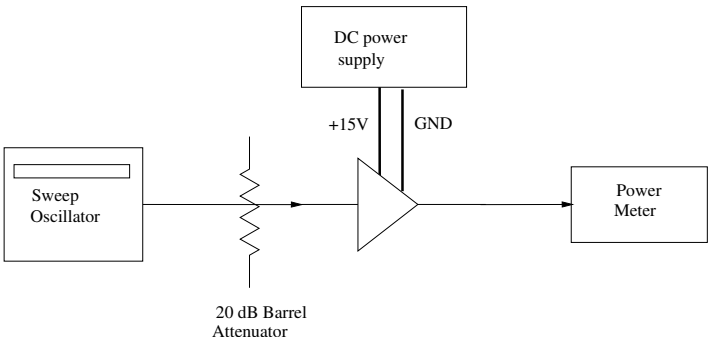

Figure 5.2: Amplifier Test Setup

The equipments are setup as shown in Figure 5.2. The sweep oscillator is first connected to the power meter which has an accuracy of $\pm 1\%$ of full scale and the power level is noted when the meter is used at a 10 dBm full scale reading. The signal is padded with a 20$\pm$0.5 dB barrel attenuator and the power out of the attenuator is measured again with the power meter. Finally, the signal, attenuator and amplifier are connected in line and the output of the amplifier is measured on the power meter at 158 MHz. The DC input voltage of the amplifiers is set to $+15\,V$ using the digital mulitimeter.

Results:

Table 5.2 shows the gain of the measured amplifier gain.

Table 5.2: ZFL-500HLN Amplifier Output Level and Gain

Amplifier	Swp. Osc. O/P [dBm]	Attn. O/P [dBm]	Amp. O/P [dBm]	Meaured Gain [dB]
AMP6	0.0$\pm$0.1	-20$\pm$0.5	0.4$\pm$0.1	20.4$\pm$0.5
AMP7	0.0$\pm$0.1	-20$\pm$0.5	0.3$\pm$0.1	20.3$\pm$0.5
AMP8	0.0$\pm$0.1	-20$\pm$0.5	0.2$\pm$0.1	20.2$\pm$0.5
AMP9	0.0$\pm$0.1	-20$\pm$0.5	0.3$\pm$0.1	20.3$\pm$0.5

5.2.2 2^{nd} IF Amplifier Test

The setup used in Section 5.2.1 is repeated for the amplifier in the 2^{nd} IF stage. Table 5.3 shows the expected properties of the amplifier as specified in the data sheet.

Table 5.3: Properties of ZEL-1217LN Amplifier

Amplifier	Noise Figure [dB]	Gain [dB]	DC Voltage [V]	Current [mA]	1 dB pt [dBm]
AMP5	1.5	25	+15	70	+10

Test:

The equipments are setup exactly as in Figure 5.2 and the procedure is performed as explained in Section 5.2.1 with the input signal set to 0 dBm and padded by a 20±0.5 dB attenuator. The signal from the sweep oscillator, the attenuator and amplifier are connected in line and output of the amplifier, AMP5, is measured by the power meter.

Results:

Table 5.4 shows the measured gain of the amplifier, AMP5, in the 2^{nd} IF stage. A gain of 25.8 dB was achieved with DC supply of $+15V$.

Table 5.4: ZEL-1217LN Amplifier Output Level and Gain

Swp. Osc. O/P [dBm]	Attn. O/P [dBm]	Amp. O/P [dBm]	Meaured Gain [dB]
-4.0±0.1	-24±0.5	1.80±0.1	25.8±0.5

5.2.3 3^{rd} IF Amplifier Test

The *Low Noise Amplifier* (LNA) is essential in setting the front-end noise figure. The datasheet specifies the following properties as listed in Table 5.5.

Table 5.5: LNA Properties

Amplifier	Noise Figure [dB]	Min. Gain	DC Voltage [V]	Current [mA]	1 dB pt. [dBm]
LNA	0.9	20	+15	150	+10

Equipment Required:

Sweep Oscillator, DC Power Supply, INMET Barrel Attenuators, Power Meter, Digital Multimeter, Test Cables.

Test:

The test setup is similar to the one described in Section 5.2.1. The calibrated attenuated signal is fed in the LNA at -20 dBm well below the 1-dB compression point and the output of the LNA (AMP4) is measured using the power meter.

Result:

The output was measured using the power meter and Table 5.6 shows the result.

Table 5.6: LNA Test Result

Sweep Osc. O/P [dBm]	Attenuator O/P [dBm]	Amp. O/P [dBm]	Meaured Gain [dB]
0.0±0.1	-20±0.5	1.6±0.1	21.6±0.5

5.3 The MGC Unit

The MGC is made up of the following 4 components:

1. 3-bit digital attenuator.
2. Bandpass filter.
3. Amplifiers.
4. Two-way splitter.

5.3.1 Insertion Loss

This test determines the loss in the MGC subsection when a signal is fed through the one port from the sweep oscillator and the output is measured using the power meter.

Equipment Required:

Sweep Oscillator, DC Power Supply, INMET Barrel Attenuator (10 ± 0.5), Spectrum Analyser, Power Meter, Coaxial Cables (Test Cables).

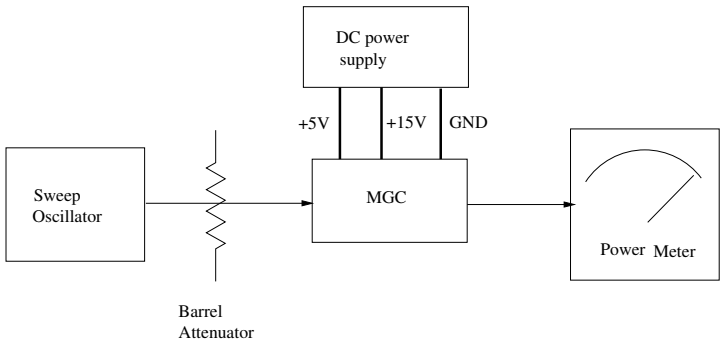

Figure 5.3: MGC test setup

Test:

The test is setup as shown in Figure 5.3. The sweep oscillator is connected to the attenuator via coaxial. The power output of the oscillator is set using the power meter and the frequency of the signal is monitored on the spectrum analyser before injecting the signal in the MGC unit. For a 10 ± 0.5 dB barrel attenuator, this ensures that the power at the attenuator output is set to -13.9 ± 0.5 dBm, at a frequency of 158 MHz, with losses in the cable not incorporated in the test measurements.

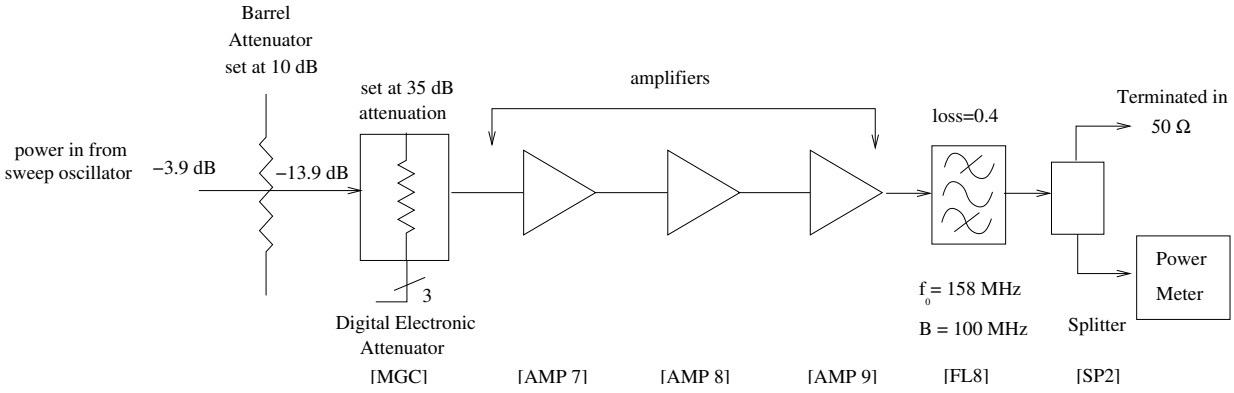

Figure 5.4: Initial MGC Components Setup

The components are then interconnected with the output of the splitter, SP2, connected to the power meter as shown in Figure 5.4 and the power level of the 158 MHz response is measured.

The initial setup of Figure 5.4 was changed to that of Figure 5.5 in order to suppress the distortion that occurred.

Results:

The output displayed on the spectrum analyser contained harmonics in the passband that were generated and amplified by 60.8 dB. The power level at certain points in the MGC

line together with the output power level at the splitter, SP2, is shown in Figure 5.5 with power level being below the 1-dB compression point of the amplifiers.

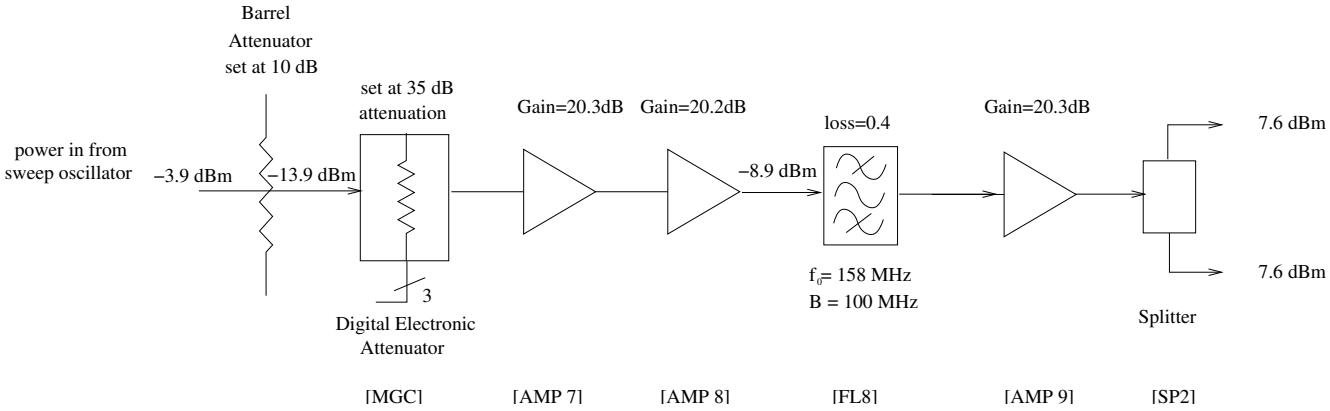

Figure 5.5: Final MGC Setup with Power Level Indicated

Table 5.7 shows the output of the MGC stage with the expected output as can be inferred from Table B.1 of Appendix B.

Table 5.7: Input and Output Power Level of MGC Stage

Stages	MGC Input [dBm]	Splitter SP2 Output [dBm]	Expected Output [dBm]
Power Level	-13.9 ± 0.5	7.6 ± 0.1	7.02

Figure 5.6 shows the input signal as measured on the spectrum analyser and the measured output is shown in Figure 5.7. Figure 5.8 shows the output, displayed on the spectrum analyser, as measured with the initial arrangement shown in Figure 5.4.

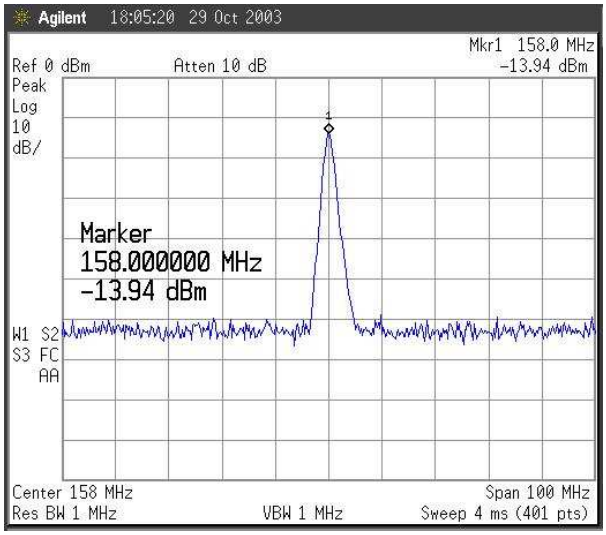

Figure 5.6: MGC Input Signal Level

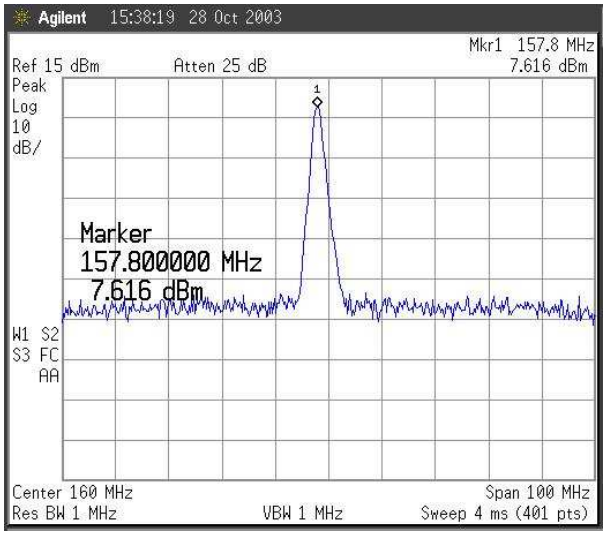

Figure 5.7: MGC Signal Output Level

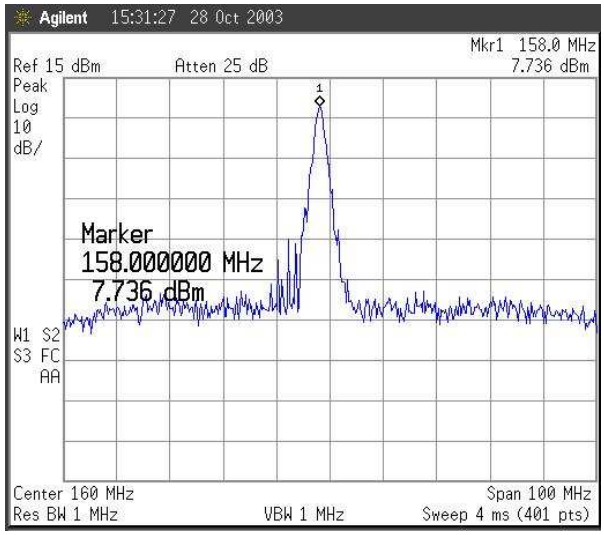

Figure 5.8: MGC Output without Amplifier Padding

5.3.2 MGC Frequency Response

This test is to determine the combined effect of the filter with the MGC components.

Test:

The test equipments are setup exactly as shown in Figure 5.5 with an attenuated input signal of -13.9 ± 0.5 dBm at 158 MHz. The frequency of the sweep oscillator is then varied. The power level of each of these frequency spectra is measured at the output of splitter SP2.

Results:

The expected 3-dB bandwidth for the filter in the MGC section is 100 MHz. Figure 5.9 shows the filter transfer function. The 158 MHz has a relative gain of 21.5 dBm. Table 5.8 shows the power level as measured by the power meter. The last column shows the relative gain of each spectrum as the input signal was varied. This allows cancelation of any non-linearities in the sweep oscillator amplitude.

Table 5.8: Output Level of MGC Unit at SP2

Freq. [MHz]	P_{IN} [dBm]	$P_{IF} + G$ [dBm]	Rel. Gain [dB]
90.8	-13.9	-6	7.9
108	-13.9	4.6	18.5
158	-13.9	7.6	21.5
208	-13.9	5.3	19.2
218	-13.9	0.4	14.3
234.6	-13.9	-6	7.9

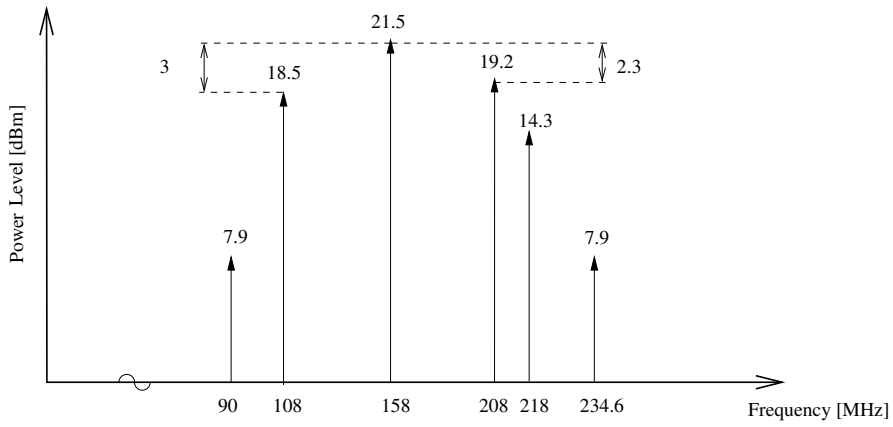

Figure 5.9: Relative Gain of MGC Output at FL8

5.4 The STC Unit

The STC is composed of 4 components namely:

1. *Single pole double throw* (SPDT) switch.
2. Bandpass filter.
3. Electronic attenuator.
4. Amplifier.

5.4.1 Insertion Loss

As explained in Section 5.3.1, this test investigates the insertion loss of the STC subsection of the 1^{st} IF at 158 MHz.

Equipment Required:

Sweep Oscillator, DC power supply, INMET Barrel Attenuators (10$\pm$0.5 dB), Spectrum Analyser, Power Meter, Coaxial Cables (Test Cables).

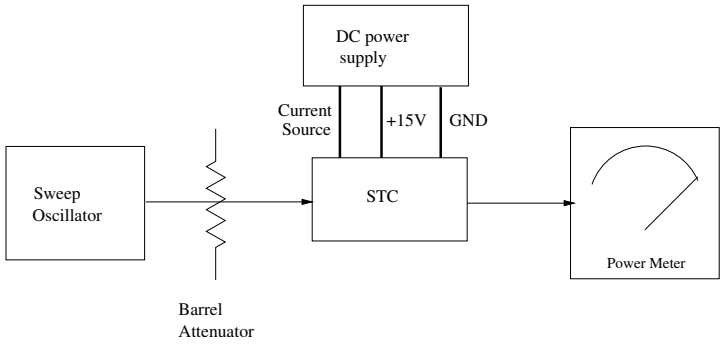

Figure 5.10: STC Test Setup

Test:

The test is setup as shown in Figure 5.10. The sweep oscillator is connected to the attenuator via the coaxial test cable. The power output of the oscillator is calibrated using the power meter which has a 1% uncertainty. The frequency of the signal is monitored on the spectrum analyser before injecting in the STC unit. This ensures that the power at the attenuator output is set to -12.7 ± 0.5 dBm, at a frequency of 158 MHz. The signal level of -12.7 dBm is chosen to ensure that the amplifier is well below the compression point as can be inferred from Table B.1 of Appendix B.

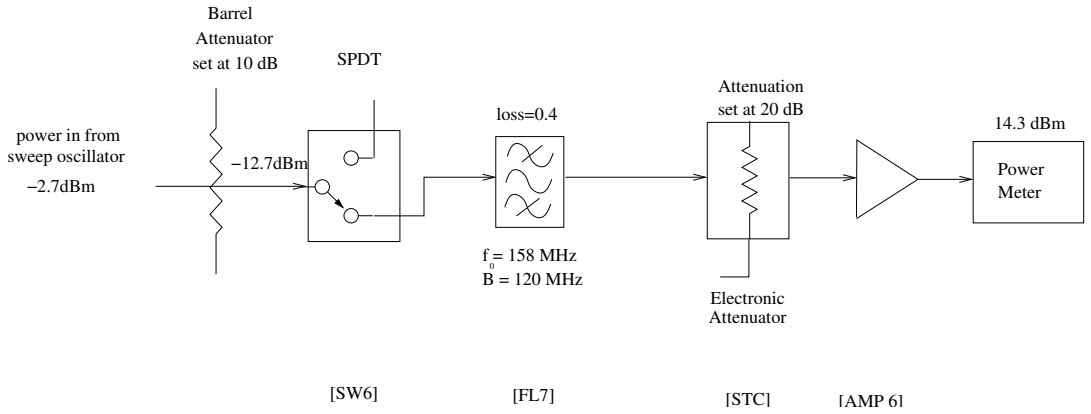

Figure 5.11: STC Components Test Setup

The components are then interconnected with the output of the amplifier connected to the power meter as shown in Figure 5.11 and the power level of the 158 MHz response is measured.

Results:

The output measured by the power meter for a full scale reading of 20 dBm is -14.3±0.2 dBm as laid out in Table 5.9.

Table 5.9: Table Showing Input and Output Power Level of STC Stage

Stages	STC Input [dBm]	AMP6 Output [dBm]	Expected Output [dBm]
Power Level	-12.7 ± 0.5	-14.3 ± 0.2	-13.9

5.4.2 STC Frequency Response

Test:

The test equipments are setup as shown in Section 5.4.1. The sweep oscillator frequency is varied at constant power level and the frequency response is measured for definite frequencies of interest. The STC filter has a specified 3-dB bandwidth of 120 MHz and the actual 3-dB bandwidth is measured from this test.

Results:

The characteristic transfer function of the filter embedded in the STC stage is measured for frequencies of interest. Table 5.10 shows the relative gain of the amplifier, AMP6, from an input signal at 158 MHz and the cut-off effect of filter, FL7, as the frequency of the input signal is varied.

Figure 5.12 shows the output at the amplifier, AMP6, as measured by the power meter.

Table 5.10: Output Level of STC Unit at AMP6

Freq. [MHz]	P_{IN} [dBm]	$P_{IF} + G$ [dBm]	Rel. Gain [dB]
83.5	-12.4	-23.8	-11.4
98	-12.7	-17.3	-4.6
158	-12.7	-14.3	-1.6
218	-12.7	-17.6	-4.9
246	-12.7	-23.8	-11.1

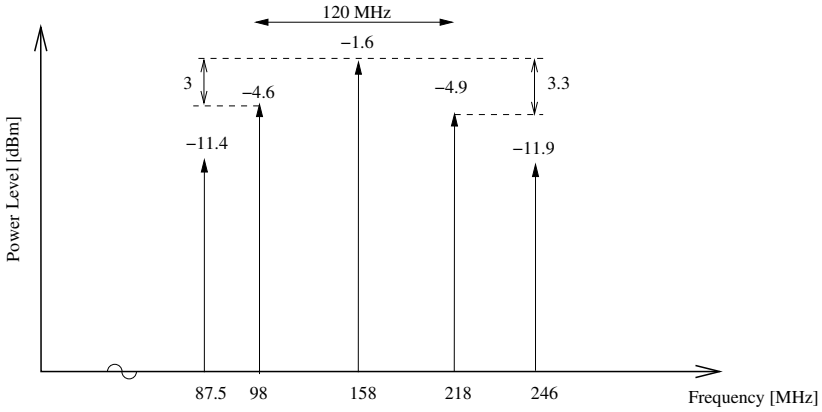

Figure 5.12: STC Filter Transfer Function

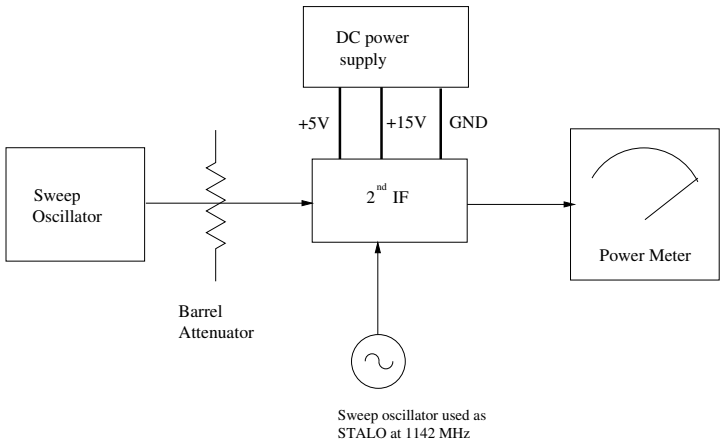

Figure 5.13: 2^{nd} IF Test Setup

5.5 The 2^{nd} IF Unit

5.5.1 Insertion Loss

This test is applied to the 2^{nd} IF unit to ensure proper functioning of the components. A signal of -32.7 ± 0.8 dBm is applied to the input and the frequency of the output port of the 2^{nd} IF unit is monitored on the spectrum analyser, as shown in Figure A.3 of Appendix A. The power level of the output is then measured using the power meter with full scale reading of 20 dBm. The input power level of this unit refers to the return power from a corner reflector, after having been amplified by the X-band or 3^{rd} IF section.

Equipment Required:

Sweep Oscillator, DC Power Supply, INMET Barrel Attenuators (30$\pm$0.8 dB), Spectrum Analyser, Power Meter, Coaxial Cables (Test Cables).

Test:

The test is setup as shown in Figure 5.13. The sweep oscillator is connected to the attenuator via coaxial. The power output of the sweep oscillator is set using the power meter. This ensures that the power at the attenuator output is set to -32.7 ± 0.8 dBm taking into account the specified uncertainty of a 30 dB attenuator.

The components are then interconnected as shown in Figure 5.14 and the power level of the 158 MHz response is measured using the power meter at the output of mixer, M6.

Results:

The output is measured by the power meter as -15.2 ± 0.2 dBm for a full scale reading of 20 dBm. Table 5.11 shows the input and output signal level through the 2^{nd} IF as measured by the power meter and the corresponding expected output level. The expected

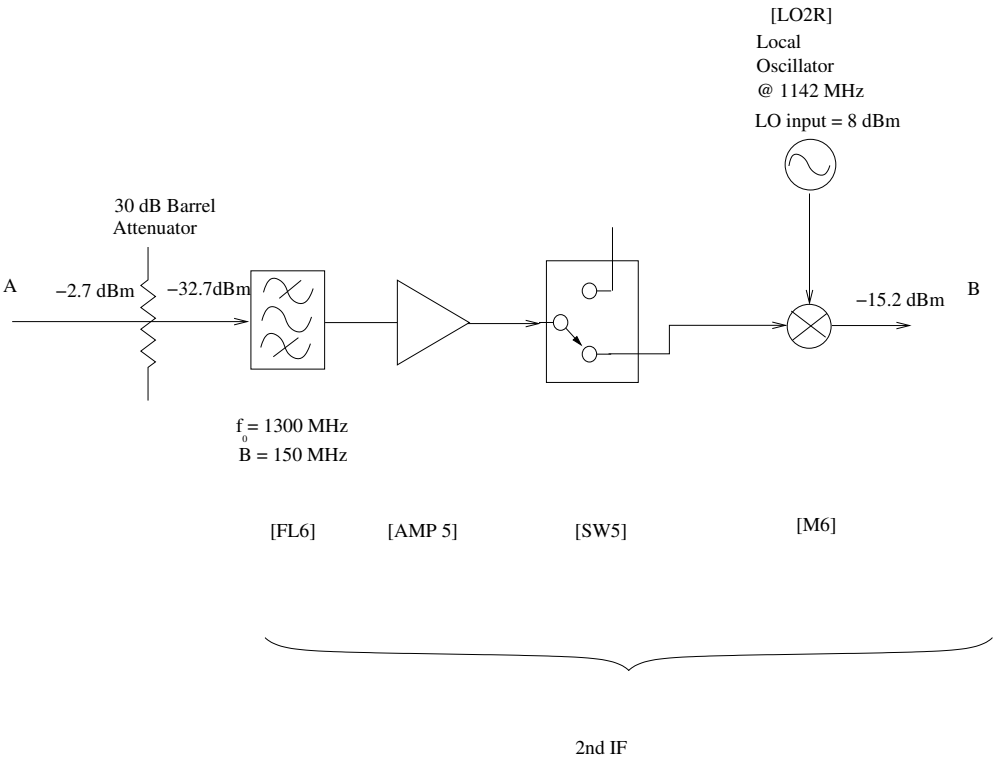

Figure 5.14: 2^{nd} IF Components Schematic

output is higher by 2.5 dB probably due to an underestimate in the losses in the cabling and the components used.

Table 5.11: Table Showing Input and Output Power Level of 2^{nd} IF Stage

Stages	P_{IN} [dBm]	P_{OUT} [dBm]	Expected Output [dBm]
Power Level	-32.7 ± 0.8	-15.2 ± 0.2	-12.7

Figures 5.15 shows the frequency response with the marker on the 1142 MHz input signal, which is the LO signal, attenuated by the combined effect of the mixer and filter to -15.2 dBm from 10.4 dBm.

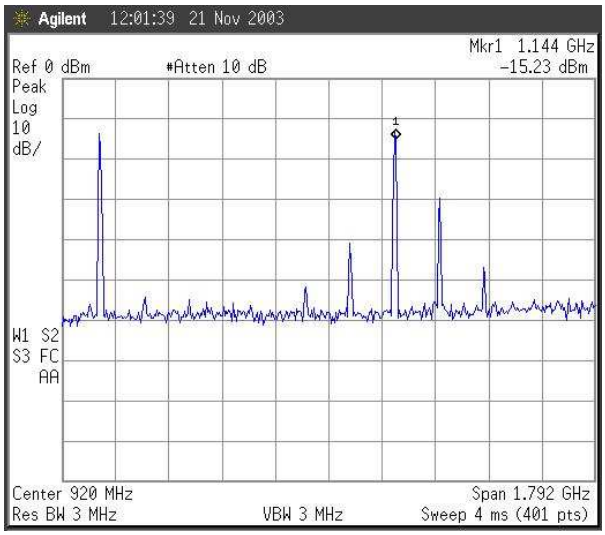

Figure 5.15: 2^{nd} IF Frequency Response

5.5.2 2^{nd} IF Frequency Response

Test:

The test equipments are setup as in Section 5.5.1. The sweep oscillator frequency is varied and the frequency response is measured for definite frequencies of interest. The expected filter 3-dB bandwidth is 150 MHz.

Result:

Table 5.12 shows the power level of the output signal, as measured by the power meter. Figure 5.16 shows the measured output at the mixer, M6, with the input frequency being manually swept from 1207 MHz to 1404 MHz, and the stable LO being fixed at 1142 MHz.

Table 5.12: Output Level of 2^{nd} IF unit at M5

Freq. [MHz]	Swp Osc. [dBm]	$P_{IF} + G$ [dBm]	Rel. Gain [dB]
65	-32.7	-26.2	6.5
81	-32.7	-18.2	14.5
158	-32.7	-15.2	17.5
233	-32.7	-17.3	15.4
262	-32.7	-28.5	4.2

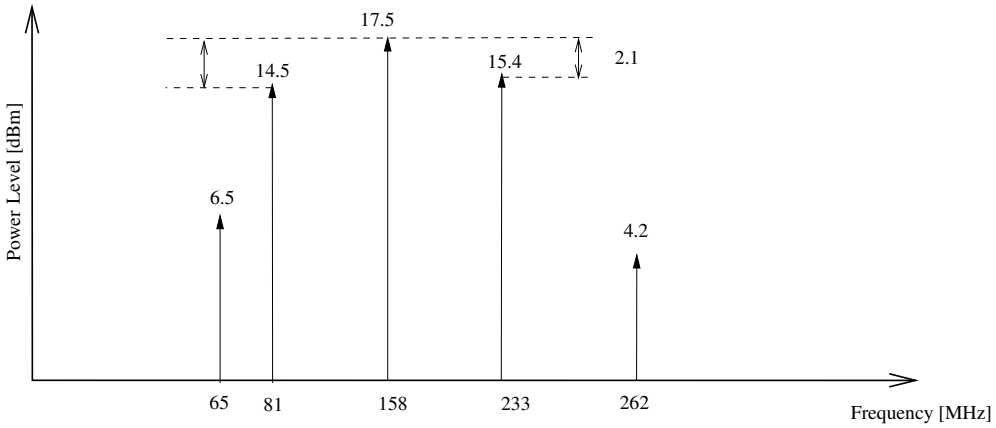

Figure 5.16: Relative Gain of 2^{nd} IF Output Signal.

5.6 The 3^{rd} IF

5.6.1 Insertion Loss

Equipment Required:

Sweep Oscillator, DC power supply, INMET barrel attenuators (20 ± 0.5 dB, 30 ± 0.8 dB), spectrum analyser, power meter, Coaxial Cables (Test Cables).

Test:

The equipment is setup as shown in Figure 5.17. The input to the attenuator is measured by the power meter as 0±0.2 dBm. The input to the filter is padded down set to -50 ± 0.9 dBm by two cascaded barrel attenuators where the uncertainty is given as,

$$\begin{aligned} Uncertainty &= \sqrt{0.5^2 + 0.75^2} \\ &= 0.9 \end{aligned}$$

This power level corresponds to the simulated return power from a corner reflector at the antenna output as explained in Chapter 3.

Result:

The input signal level is shown in Figure A.4 of Appendix A and the amplified and filtered output level of -34.6 ± 0.4 dBm is measured using the power meter for a full scale reading of 30 dBm. Table 5.13 shows the input and output signal level through the 3^{rd} IF unit and the corresponding expected output level. The output level is comparable with the expected output. The 1.9 dB difference is due to an underestimate of the losses in the componentes and cabling of the 3^{rd} IF subsystem.

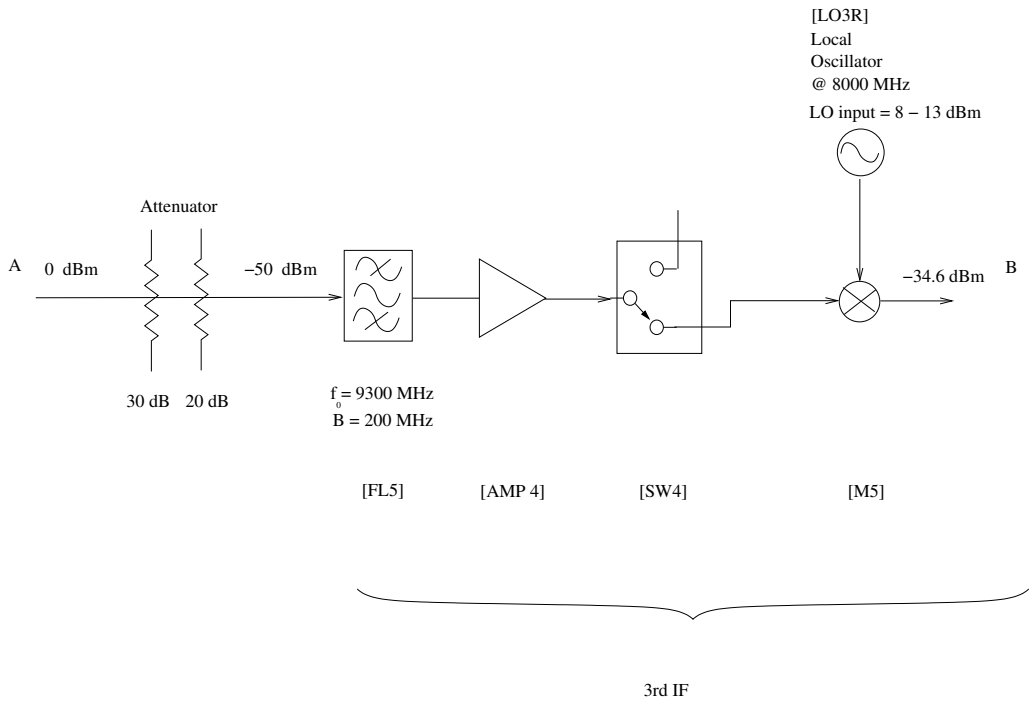

Figure 5.17: X-Band Test Setup

Table 5.13: Input and Output Power Level of 3^{rd} IF Stage

Stages	3^{rd} IF Input [dBm]	Output [dBm]	Expected Output [dBm]
Power Level	-50 ± 0.9	-34.6 ± 0.4	-32.7

5.6.2 3^{rd} IF Frequency Response

Test:

The test setup of Section 5.6.1 is used to test the cut-off effect of the filter FL5 of the 3^{rd} IF as the input frequency is manually swept. The input frequency is swept over a range of frequencies and the output of the mixer M5 is measured using the power meter. The spectrum analyser is used to display the spectrum before measurement to ascertain that unwanted oscillation is not creeping through. The stable LO was set to 8000 MHz at a power level of 10 dBm and monitored throughout the experiment.

Results:

Table 5.14 shows the output level as the frequency of the input spectrum was varied manually. The expected 3-dB bandwidth of the filter FL5 is 200 MHz. Figure 5.18 shows the reponse of the 3^{rd} IF. The 9198 MHz and 9405 MHz signals, which downconvert to a 2^{nd}

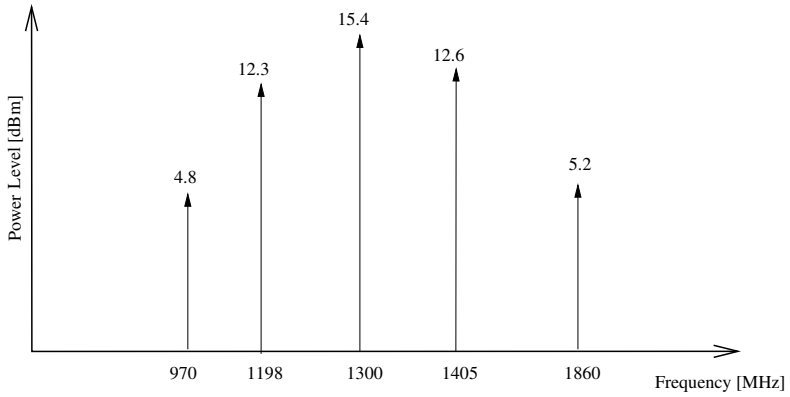

Figure 5.18: Filter Transfer Function of 3^{rd} IF

IF of 1098 MHz and 1505 MHz respectively, have respective power levels of 3.1 dBm and 2.8 dBm below the center frequency of 1300 MHz.

Table 5.14: Output Level of 3^{rd} IF unit at M5

Freq. [MHz]	Swp Osc. [dBm]	$P_{IF} + G$ [dBm]	Rel. Gain [dB]
970	-50	-45.2	4.8
1198	-50	-37.7	12.3
1300	-50	-34.6	15.4
1405	-50	-37.4	12.6
1860	-50	-44.8	5.2

5.7 Noise Figure Test

The noise figure test is performed to verify the theoretical overall noise figure of the receiver, based on the specified values of the components given in their respective data sheets. The noise meter also gives an indication of the gain of the receiver as an output result.

Equipment Required:

Noise Source, Noise Source Analyser, Sweep Oscillator, DC power supply, INMET barrel attenuators, Digital Multimeter, Test Cables.

Test:

The noise source was first calibrated using the Noise Source Analyser. The noise was injected at the input of the waveguide filter and the output of the power splitter, SP2, is measured using the noise figure meter, as shown in Figure 5.19.

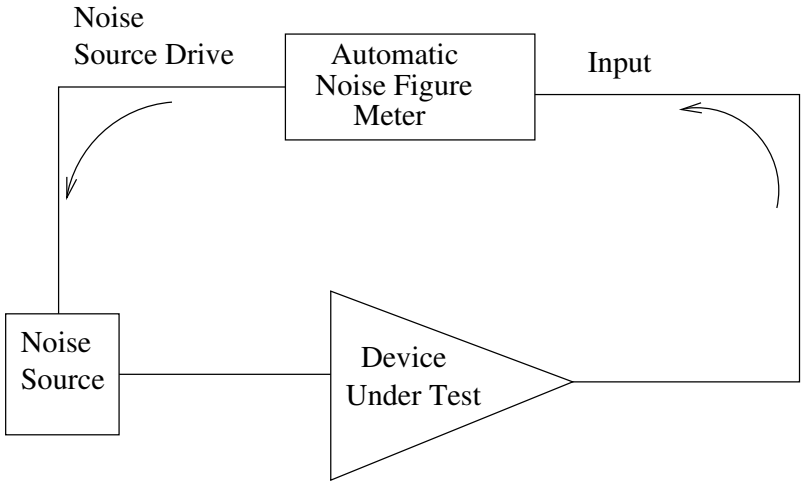

Figure 5.19: Noise Figure Test

Results:

The noise figure was calculated for a range of frequencies over a bandwidth of 500 MHz and Figure 5.20 shows the measured noise figure of the receiver.

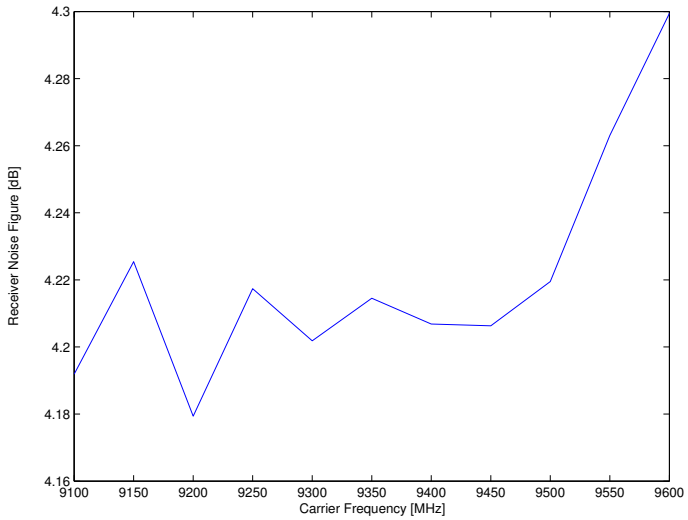

Figure 5.20: Plot of Receiver Noise Figure Test

A noise figure of 4.20 dB was measured at 9300 MHz and this corresponds to the minimum attenuation of the MGC which was set to 5 dB. The overall gain of the receiver is a secondary result of the noise meter. Figure 5.21 shows a plot of gain with frequency. The total gain of the receiver at 9300 MHz is 80.5 dB. From Table 4.1 of Chapter 4, the total gain of the receiver measured is close to the theoretical gain of 84.8 dB. This discrepancy is due to an underestimate in the losses in the receiver as cabling losses were not considered in the design.

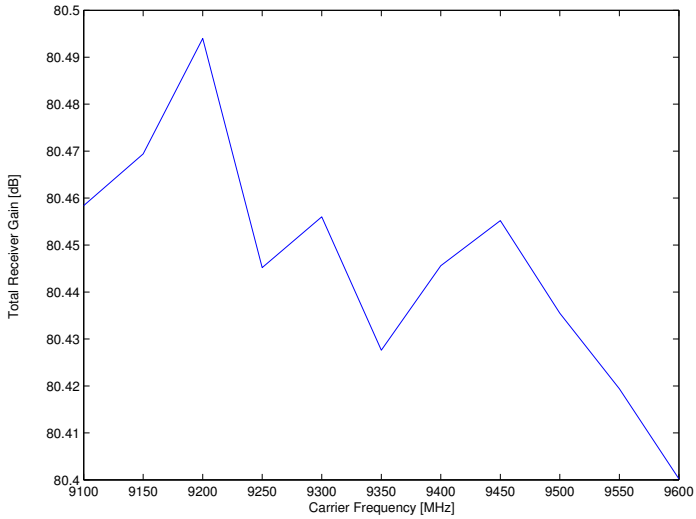

Figure 5.21: Plot of Overall Gain of Receiver (Min. Attenuation)

This noise figure relates to the system noise temperature, T_e, and is given by,

$$T_e = (F-1) \times T_\circ \tag{5.1}$$
$$= \left(10^{0.4202} - 1\right) \times 290 \tag{5.2}$$
$$= 473\,\mathrm{K} \tag{5.3}$$

where F is the noise factor.

The worst-case noise figure is attained when the MGC is switched on to maximum attenuation of 35 dB when large targets are expected in the swath width. Figure 5.22 shows the noise figure of the receiver over a 500-MHz bandwidth. The worst-case measured noise figure at 9300 MHz sits at 9 dB resulting in a noise temperature given by,

$$T_e = (10^{0.9} - 1) \times 290 \tag{5.4}$$
$$= 2014\,K \tag{5.5}$$

Figure 5.23 shows a plot of the calculated cumulative noise figure down the receiver chain. The output noise figure of the LNA is plotted up to the output of the splitter, SP2. An overall noise figure of 2.47 dB is expected at minimum attenuation. This results in a

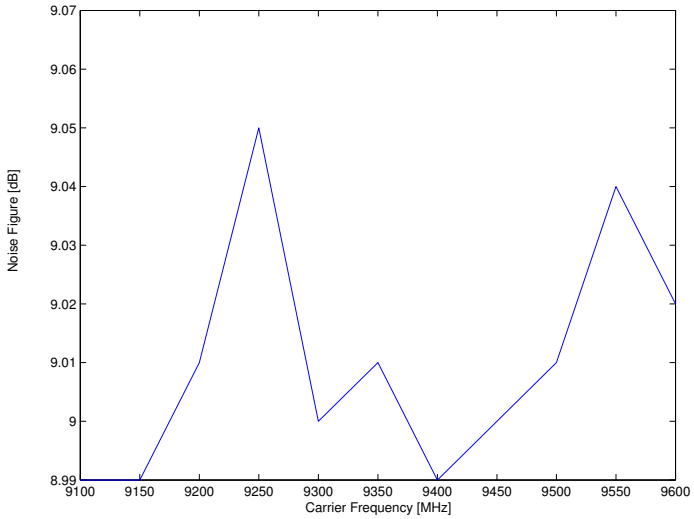

Figure 5.22: Worst-Case Noise Figure

theoretical receiver noise temperature given by Equation 5.1 as,

$$T_e = \left(10^{0.247} - 1\right) \times 290 \tag{5.6}$$

$$= 222.2\,K \tag{5.7}$$

$$\approx 222\,K \tag{5.8}$$

The best-case noise figure measured differs by 1.73 dB whilst the worst-case noise figure is 1.54 dB higher than expected. This is probably due to a higher loss in power in the receiver components and cabling.

5.8 Bandwidth Test

The cascaded filters are tested in this section to verify the cut-off frequency and the -3-dB spectrum on either side of the centre frequency of 158 MHz.

Equipment Required:

Sweep Oscillators, DC power supply, INMET barrel attenuators, Digital Multimeter, Spectrum Analyser, Test Cables.

Test:

The experiment was setup as shown in Figure 5.24. The input and the two LO's were fed from 3 calibrated sweep oscillators. The frequency of the input signal was then swept over a bandwidth of 200 MHz with the centre frequency being at 9300 MHz. The peak of the downconverted signal was measured and displayed using the spectrum analyser.

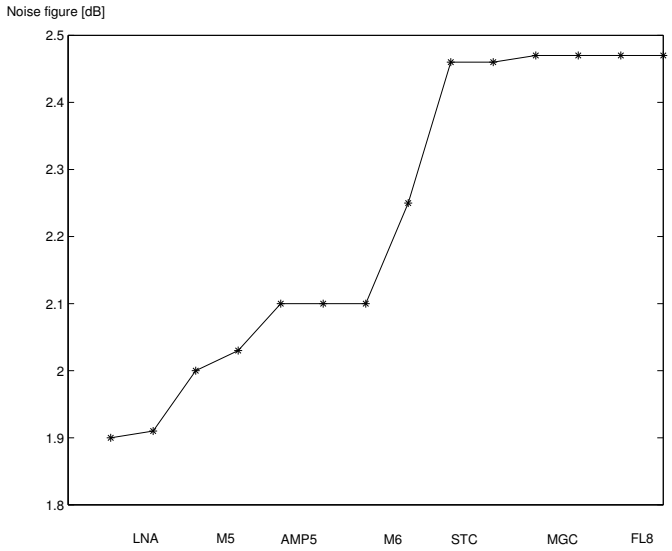

Figure 5.23: Theoretical Plot of Noise Figure of the Receiver (Min. Attenuation)

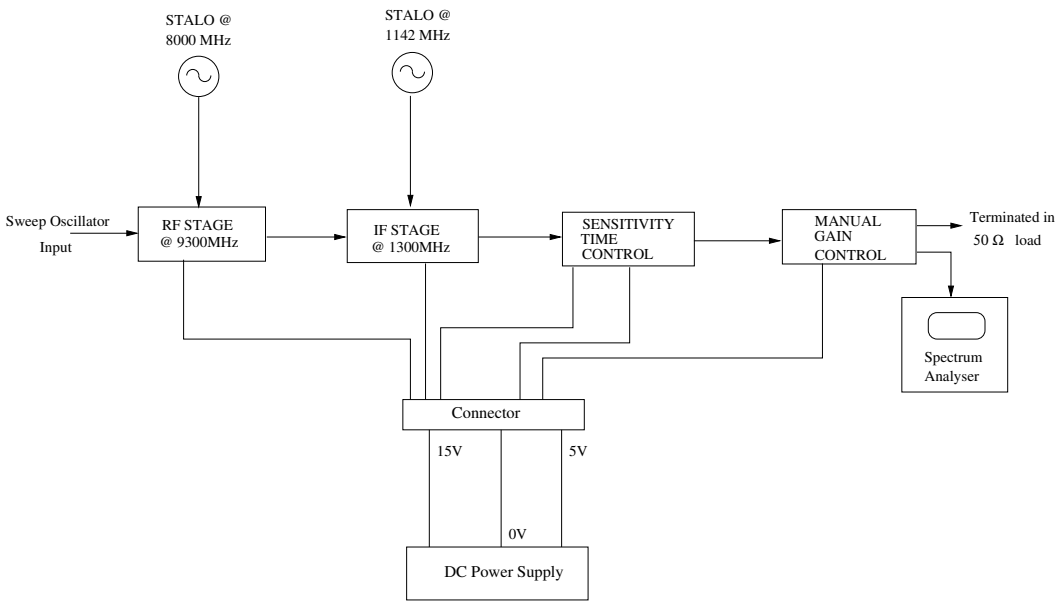

Figure 5.24: Receiver Test Setup

Table 5.15: Spectral Power Level Relative To The Centre Frequency

Frequency [MHz]	Power Level [dBm]	Rel. Power Level to Centre Freq. [dBm]
98	-11.98	-10
108	-4.98	-3
158	-1.98	0
202	-4.97	-2.99
216.5	-11.98	-10

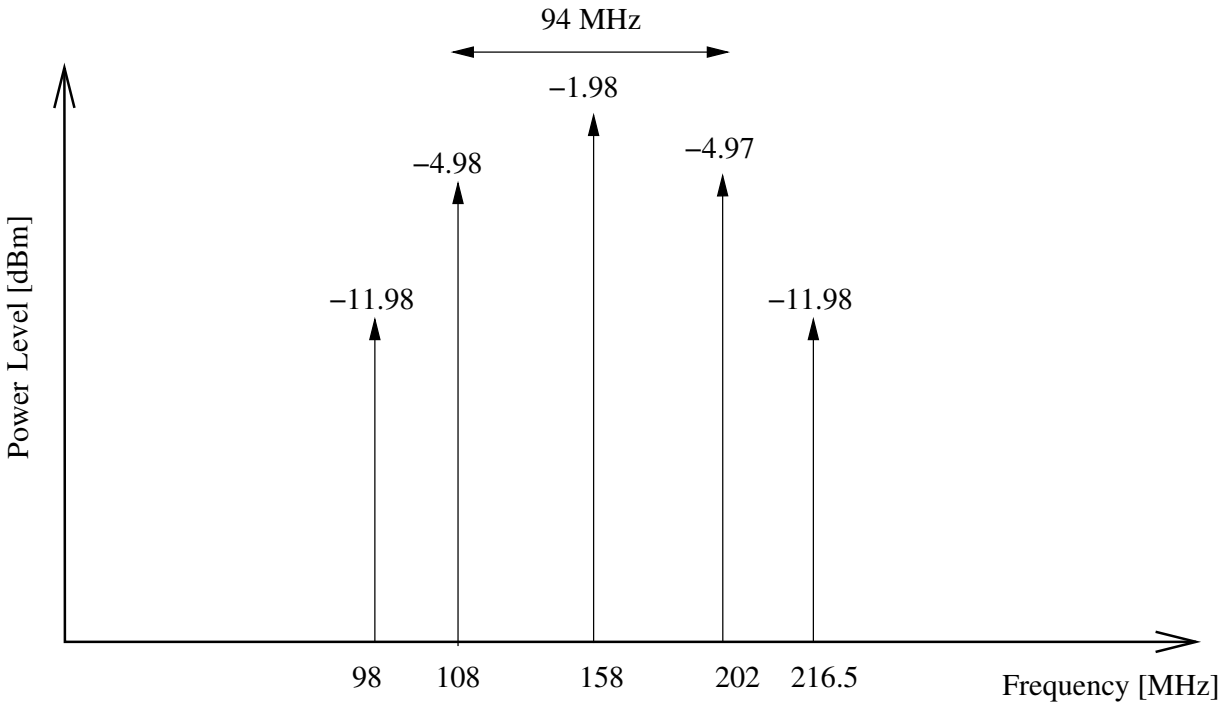

Figure 5.25: Relative Spectral Power Level

Results:

From the spectrum analyser, a marker was fixed on the centre IF of 158 MHz at -1.98 dBm and a second marker was used to read off the different spectral power level relative to the centre frequency and the result is tabulated in Table 5.15.

Figure 5.25 shows the relative spectral power level of the downconverted signal, from 9300 MHz to 158 MHz, with an overall -3-dB bandwidth of 94 MHz. This is 6 dB short of the resultant 3-dB bandwidth of 100 MHz that the receiver was designed for. Figure 5.26 shows the output as displayed on the spectrum analyser with the second marker on the -3-dB signal relative to the centre frequency.

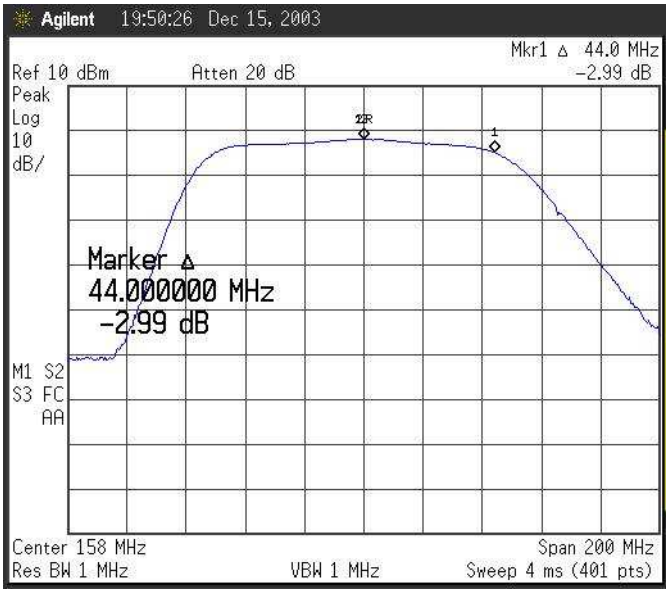

Figure 5.26: Receiver Transfer Function Displayed Spectrum Analyser

5.9 Summary

The tests performed in this chapter are to verify the design of the receiver. The best-case and worst-case scenarios were tested. The receiver was broken down into 4 stages and the tests performed are listed below:

- Amplifier Gain Test.

  This test was used to verify the actual gain of the amplifiers used.

- Insertion loss tests of the four stages of receiver namely,

1. MGC section.
2. STC section.
3. 2^{nd} IF section.
4. 3^{rd} IF section.

   The tests include the input of a signal at a power level designed in Table B.1 of Appendix B for the different IF sections and measuring the output power level. The frequency of the input signal is manually varied and the filter transfer function is verified and the actual 3-dB bandwidth is measured.

Table 5.16: Output and Expected Power Level

Section	Input Power [dBm]	Output Power [dBm]	Expected Output Power [dBm]
3^{rd} IF	- 50	- 34.6	- 32.7
2^{nd} IF	- 32.7	- 15.2	- 12.7
STC	- 12.7	- 14.3	- 13.9
MGC	- 13.9	7.6	7.02

- Receiver noise figure test.

  The theoretical noise figure of the receiver is tested for both the best-case and worst-case scenario. A noise figure of 4.20 dB is measured at minimum attenuation of the MGC.

- Receiver Frequency Response

  The frequency of the input signal is varied over a bandwidth of 200 MHz, with the centre frequency at 9300 MHz, and the transfer function of the combined filters is measured to be 94 MHz.

Chapter 6

Conclusions and Recommendations

Based on the design and tests results of this dissertation and the experience gained in designing this receiver, the following conclusions can be drawn:

- A receiver gain of 60 dB is sufficient in boosting the largest signal to within the operating input power of the ADC. An input power of - 50 dBm resulted in a receiver output of -1.98 dBm. The expected output power of the receiver was 7.06 dBm. Losses in the cabling and connectors, and filtering are the main contributing factors in attenuating the signal to -1.98 dBm.
- The amplifiers are within the manufacturers' specifications. The DC supply voltage was kept to $+15\,V$. Table 6.1 shows the different amplifiers used in the receiver and their respective expected and measured gain.
- The transfer functions of the bandpass filters are adequate in attenuating spurious responses, while allowing the required RF signal to pass. A series of 4 cascaded filters were designed to attain a final 3-dB bandwidth of 100 MHz. The measured 3-dB bandwidth of the receiver is 94 MHz.

Table 6.1: Expected and Measured Amplifier Gain.

Amplifier	Expected Min. Gain [dB]	Measured Gain [dB]
AMP4	22	21.5
AMP5	25	25.8
AMP6	19	20.4
AMP7	19	20.3
AMP8	19	20.2
AMP9	19	20.3

- The dual downconversion ensures that spurious responses are attenuated by the filters from the 3rd to the 1st IF. The attenuation of the stable LO for the 2^{nd} IF, is measured to be 25.6 dB, which is due to the rejection property of mixer, M6. This ensures that the 1142 MHz stable LO creeping through to the next stage, will be attenuated further down through the use of the 1^{st} IF filters to reach a minimum.

- Placing the antenna boresight axis closer to the far-swath, helps in boosting the return power from targets falling in the 3-dB beamwidth at the far range. The drop in the power level of the targets at near-swath, is small and is due to the fact that the targets at near range fall outside the 3-dB beamwidth.

- The quantisation noise is 15.4 dB below the thermal noise for maximum attenuation of the MGC, hence allowing for signal integration in post processing. Maximum attenuation occurs when large targets, e.g. corner reflector, are expected to fall in the 3-dB beamwidth of the antenna.

- The minimum noise equivalent sigma zero of the receiver, for an antenna with the mainbeam close to the far-swath, is -54.5 dB at an incidence angle of 55°.

- The system noise figure was measured to be 4.20 dB, resulting in a noise temperature of 473 K. This is achieved with a minimum attenuation of the MGC.

- None of the components are driven into saturation. The receiver works well in downconverting signals from RF of 9300 MHz to an IF of 158 MHz. The power level at the output of the receiver is lower than expected by 4.3 dB.

Future Work

Based on the experience gained and the conclusions drawn, the following recommendations are made:

- The receiver and the transmitter should be integrated and the dynamic range of the receiver tested. This would also allow the testing of the test loops set by the system engineer.

- To cater for the lower than expected output signal of the receiver, an additional amplication stage of 10 dB should be provided.

- The antenna section, comprising of the duplexer and TR cell, should be included in the receiver and a pre-flight demonstration of the radar should be performed to test the power reflection from the antenna and attenuation of the TR cell.

- The filter transfer function should be improved to achieve the 3-dB bandwidth of 100 MHz specified in the user requirements.

Appendix A

Spectrum Analyser Output

Figures A.1 and A.2 shows the two spectra at 3 dB below the 158 MHz centre frequency.

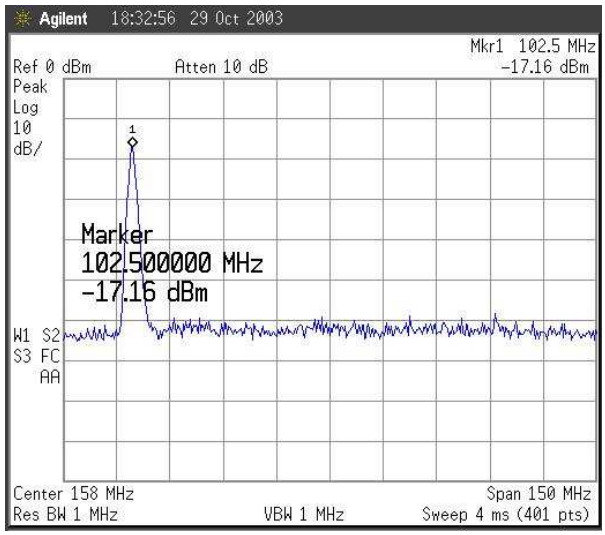

Figure A.1: Low Side Signal Level of 3-dB Filter Cut-Off.

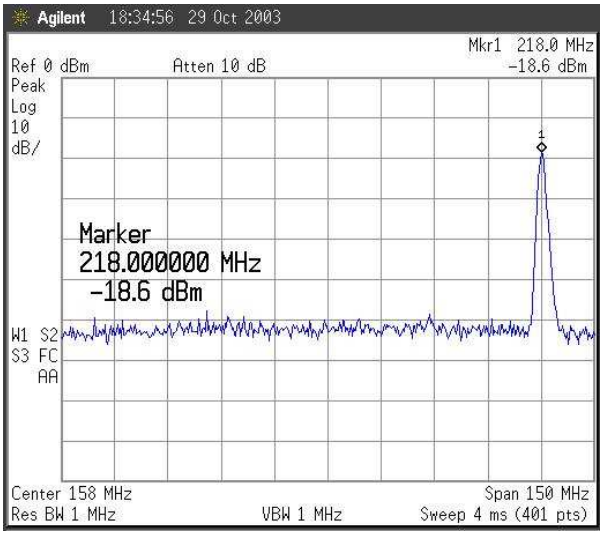

Figure A.2: High Side Signal Level of 3-dB Filter Cut-Off.

The mixer M6 output signal of the 2^{nd} IF is shown in Figure A.3 as displayed on the spectrum analyser.

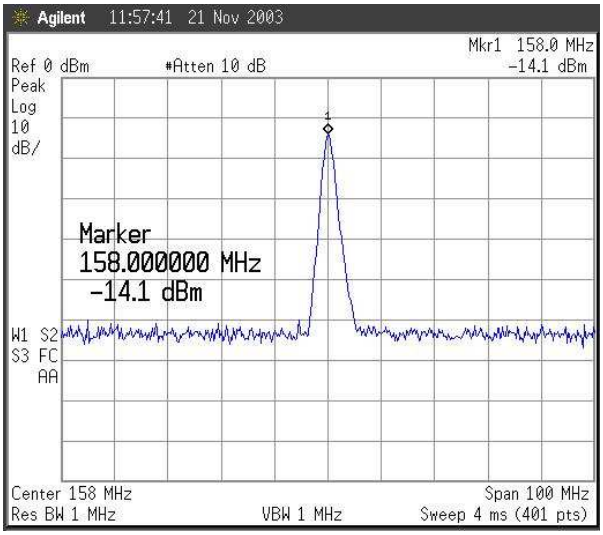

Figure A.3: Output Signal at 158 MHz

The input signal of the 3^{rd} IF stage is displayed in Figure A.4 before testing.

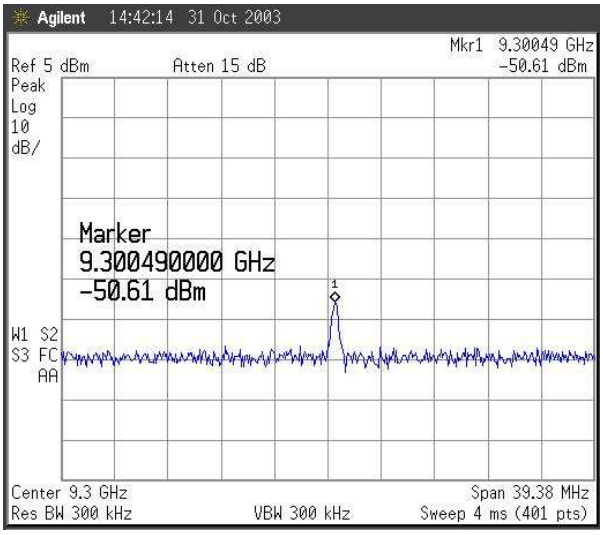

Figure A.4: Input Signal for 3^{rd} IF

The output test signal of the 3^{rd} IF stage is shown here in Figure A.5.

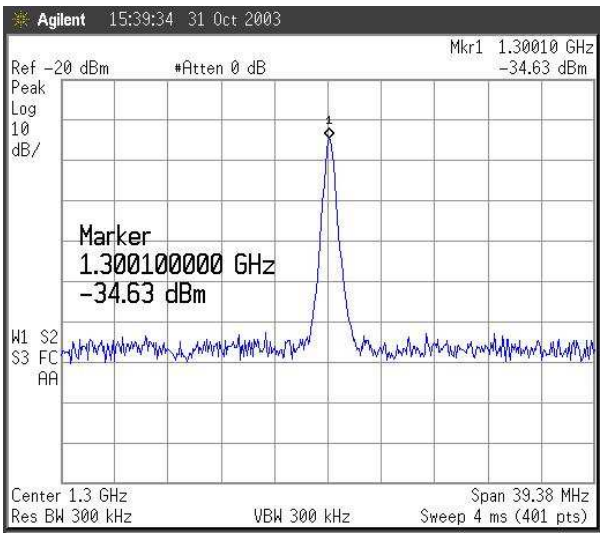

Figure A.5: Output Signal Level for 3^{rd} IF

Appendix B

Receiver Level Table For Max Attenuation

Table B.1: System Budget Calculations

Components	Input	FL5	LNA	SW4	M5	FL6	AMP5	M6	FL7	STC	AMP6	MGC	AMP7	AMP8	AMP9	FL8/SP2
Stages	1	2	3	4	5	6	7	8	9	10	11	12	13	14	15	16
Bandwidth {MHz]		200	900	18000	500	150	5000	4300	120	2000	500	1000	500	500	500	100
Noise Figure [dB]		1	0.9	1.5	6	1	1.5	7	1.2	20	3.8	35	3.8	3.8	3.8	4
Gain [dB]		-1	22	-1.5	-6	-1	28	-7	-1.2	-20	20	-35	20	20	20	-4
Cumulative Gain [dB]		-1	21	19.5	15	14	42	35	33.8	13.8	33.8	.-1.2	18.8	38.8	58.8	54.8
Signal (max) [dBm]	-50	-48.74	-26.74	-28.24	-32.74	-33.74	-5.74	-12.74	-13.94	-33.94	-13.94	-48.94	-29.94	-8.94	11.06	7.06
Noise [dBm]	-90.97	-90.97	-65.88	-67.29	-71.78	-72.76	-44.501	-51.49	-52.49	-72.09	-51.90	-82.19	-60.53	-40.52	-20.52	-24.52
1 dB compression pt. [dBm]			8		-1		10				16		16	16	16	
Cum. Noise Figure [dB]			1.9	1.91	2.00	2.03	2.10	2.10	2.10	2.25	2.46	5.59	7.94	7.96	7.96	7.96

Appendix C

Swath Width Simulation Code

```
%constant file for power return simulation
%Ajmal Mohungoo
%25/02/03
clc
h = 3000;%-------height h
c = 3e8; %-------speed of light
k =1.380658e-23;
Pt = 3500;%------Tx power
beamwidth = 30;%-3dB beamwidth degrees
%IF frequcency in GHz
IF = 0.158e9;
%Tx frequency
freq = 9.3e9 ;
lambda = c/freq;
%Losses - All system losses up to input of 1st BPF
%normal unit not dB
Loss = 10^1;
%Antenna diameter
d = 0.617; %in azimuth to achieve 3 degrees
d_ele = 0.0617; %to achieve ele beamwidth of 30
Ant_area = d*d_ele;
%Antenna Losses
eff = 0.6;
%Gain TRX Max
Gnesz = 4*pi*(Ant_area)*eff/lambda^2;
%for receiver front end
bandwidth = 200e6;
bandwidth_AD = 120e6; %sampling bandwidth
pulsewidth = 5e-6;
azi_beamwidth = 3*pi/180;
%slant range resolution
dr = c/(2*bandwidth_AD);
```

```
%range bins
R_bin = input('==>Input Range Bin (4096,8192) :');
%slant swath width
slt_swath_width = R_bin*dr;
fprintf('==>Slant Range Swath width : %d m\n', R_bin*dr)
%------User Input parameters of incidence angle and step size--------------------
%------incidence angle of near range
%------add user defined input angle
%------disp('E.g incidence angle range :25')
start_angle = input('==>Near swath incidence angle in degrees :');
gnd_range_start = h*tan(start_angle*pi/180);
slt_range_start = sqrt(h^2 + gnd_range_start^2);
%slant range from radar to near incidence
slt_range_stop = slt_range_start + slt_swath_width;
%total slant swath width
gnd_range_stop = sqrt(slt_range_stop^2 - h^2);
%converting from slant range to ground range
gnd_swath_width = gnd_range_stop - gnd_range_start; %total ground swath width
fprintf('==>Ground Range Swath Width : %g m\n',gnd_swath_width)
gnd_base_dist = gnd_range_start + gnd_swath_width;
stop_angle = 180/pi*atan(gnd_base_dist/h);
%Print swath width, beamwidth required
fprintf('==>Far swath incidence angle :%2.1f\n',stop_angle)
fprintf('==>Beamwidth required : %2.1f degrees\n',stop_angle - start_angle)
fprintf('==>Beamwidth of Horn Antenna : %2.1f degrees\n',beamwidth)
%incremental step in incidence angle from 3-dB edge of beamwidth
step = input('==>Step size in degrees (e.g. 5) :');
%finding swath centre
swath_centre = (gnd_range_stop - gnd_range_start)/2;
%ground range from nadir to swath centre
gnd_dist2sw_ctr = gnd_range_start + swath_centre;
%-----use if range bin not specified-----------------------------------
%finding the Near and Far Range to determine swath width
%Rf = h/cos(stop_angle*pi/180);
%Rn = h/cos(start_angle*pi/180);
%theta_i =stop_angle + beamwidth/2;
%output swath width
%fprintf('==>Swath width :%d',Rf-Rn/sin(theta_i*pi/180));
%--------------------------------------------------------------------------
%defines array of angle
inci_angle_deg = [start_angle:step:stop_angle];
inci_angle_rad = inci_angle_deg.*(pi/180);
gnd_range = h*tan(inci_angle_rad);
inci_angle = inci_angle_rad.*(180/pi);
grazing_angle_rad = pi/2 - inci_angle_rad;
```

```
%finding size of array
t = length(inci_angle_rad);
%Near Range depending on incidence angle
range = h./sin(grazing_angle_rad);
%Slant range resolution
dR_p = c*pulsewidth/2; %for average power
dR = c/(2*bandwidth); %for peak power
%system temperature
Ts = 630; %approx. 5 dB noise figure of receiver
%from nathanson radar design priciples pp 273
fprintf('\tChoose reflectivity (gamma) or backscatter coefficient\n')
choice = input('==>Type 1 for Gamma 2 for sigma_0 :');
if choice == 1
%use conversion to sigma zero from values of gamma obtained from Nathanson
sigmaDR = (10^-2.5)*cos(inci_angle_rad);
sigma_cult = (10^-2.2)*cos(inci_angle_rad);
sigmaWood = (10^-1.6)*cos(inci_angle_rad);
sigmaWHills = (10^-1.4)*cos(inci_angle_rad);
sigma_city = (10^-1.1)*cos(inci_angle_rad);
sigma_sea = (10^-2.0)*cos(inci_angle_rad);
elseif choice == 2
%Use values of sigma0 from skolnik graph
%sigma for different incidence angle
%from skolnik pg 12.36
% incidence angle
sigma_zero %call sigma_zero function
sigma_sea = 10.^([ -35 -36 -37 -38 -39 -40 -41 -43]./10);
end
%rcs from skolnik radar handbook
%1-bird 2-man 3-automobile, 4-truck, 5-corner reflector 6-cabin cruiser 7-road t
% x_value = [1:1:6];
corner_reflector = 4*pi*1.5^2/(3*lambda^2);
sigma_rcs = [0.001 1 100 200 corner_reflector 10 100];
%ground clutter area
Area_clutter_ave = range*azi_beamwidth*dR_p.*sec(grazing_angle_rad);
Area_clutter_pk = range*azi_beamwidth*dR.*sec(grazing_angle_rad);
```

Bibliography

[1] M. R. Inggs, “SASAR II Subsystem User Requirements”, Internal Report at RRSG-University of Cape Town, February 2003

[2] R.T. Lord, M. R. Inggs, “SASAR II Design Document”, Internal Report at RRSG-University of Cape Town, March 2003.

[3] R. Lord, “Technical Report on Noise Equivalent Sigma Zero”, Internal Report at RRSG-University of Cape Town, March 2003.

[4] M. R. Inggs, “SASAR2 Subsystem User Requirements” , Feb 2003.

[5] R. K. Moore et al., “Radar Terrain return at Near-Vertical Incidence”, Proc. IRE, February 1957.

[6] S. Kingsley and S. Quegan. “Understanding Radar Systems”, Scitech Publishing, Inc 1999.

[7] M. Skolnik, “Radar Handbook”, 2nd Edition, McGraw-Hil, Inc 1990.

[8] F. G. Stremler, “Introduction to Communication System”, 3rd Edition, Addison Wesley Publishing Company, Inc 1990.

[9] L. J. Cantafio, “Space-Based Radar Handbook”, Revised Edition, Artech House 1989.

[10] S. A. Hovanessian, “Radar System Design and Analysis” ,Artech House 1984.

[11] G. Stimson, “Introduction to Airborne Radar”, 2nd Edition, Scitech Publishing, Inc 1998.

[12] F. E. Nathanson, “Radar Design Principles”. McGraw-Hill Book Company 1969.

[13] M. Skolnik, “Introduction to radar systems”, 2nd Edition, McGraw-Hil, Inc 1980.

[14] K. Chang, “RF and Microwave Wireless Systems”, John Wiley and Sons, 2000.

[15] F. T. Ulaby, M. C. Dobson, "Handbook of Radar Scattering Statistics for Terrain", Artech House, Inc. 1989.

[16] R. K. Moore et al., "Radar Terrain Return at Near-Vertical Incidence", Proc. IRE Feb. 1957 pp228-238.

[17] M. R. Inggs, "User Requirements for SASAR II" 2003.

[18] Matt Loy, Texas Instruments, "Understanding and Enhancing Sensitivity in Receivers for Wireless Applications", Technical Brief SWRA030.

[19] H. Krauss et al. "Solid State Radio Engineering", John Wiley & sons 1980.

[20] P. Horowitz & W. Hill, "The Art of Electronics", 2nd edition Cambridge University Press 1995.

[21] http://sar-mri.openfuel.com

[22] Donald R. Wehner, "High-Resolution Radar", 2nd Edition Artech House 1994.

[23] J. Horrell, "Range-Doppler Synthetic Aperture Radar Processing at VHF Frequencies", PhD Thesis, University of Cape Town, 1999.

[24] R. Lord, "Aspects of Stepped-Frequency Processing for Low-Frequency SAR Systems", PhD Thesis, University of Cape Town, 2000

[25] "Op. Use of Civil-based SAR", http://southport.jpl.nasa.gov/reports/iwgsar/ 2_Introduction.html

[26] A. Desai, "Array-based GPR SAR simulation and image reconstruction", M.Sc. Thesis, University of Cape Town, 2002.

[27] J. L. Devore, "Probability and Statistics for Engineering and The Sciences", Duxbury Thomson Learning, 2000.

[28] RF/IF Designer's Handbook, Mini-Circuits Division of Scientific Components, 13 Neptune Avenue, Brooklyn, NY11235

[29] "Aeroflex/INMET datasheet" ,http://www.inmetcorp.com/IMPRDATT2 Watt.htm